hep-ph/0403158 IFUP–TH/2004–2

# Probing oscillations into sterile neutrinos with cosmology, astrophysics and experiments

**M. Cirelli**[1], **G. Marandella**[2], **A. Strumia**[3], **F. Vissani**[4]

[1] *Physics Department, Yale University, New Haven, USA*

[2] *Scuola Normale Superiore and INFN, Pisa, Italia*

[3] *Dipartimento di Fisica dell'Università di Pisa, Italia*

[4] *INFN, Laboratori Nazionali del Gran Sasso, Italia*



## Abstract

We perform a thorough analysis of oscillation signals generated by one extra sterile neutrino, extending previous analyses done in simple limiting cases and including the effects of established oscillations among active neutrinos. We consider the following probes: solar, atmospheric, reactor and beam neutrinos, Big-Bang Nucleosynthesis (helium-4, deuterium), Cosmic Microwave Background, Large Scale Structure, supernovæ, neutrinos from other astrophysical sources. We find no evidence for a sterile neutrino in present data, identify the still allowed regions, and study which future experiments can best probe them: sub-MeV solar experiments, more precise studies of CMB or BBN, future supernova explosions, etc. We discuss how the LSND hint is strongly disfavoured by the constraints of (standard) cosmology.

[1] e-mail: Marco.Cirelli@yale.edu
[2] e-mail: Guido.Marandella@sns.it
[3] e-mail: Alessandro.Strumia@df.unipi.it
[4] e-mail: Francesco.Vissani@lngs.infn.it

# Contents

**1 Introduction** **1**

**2 Active/sterile neutrino mixing** **3**
2.1 Parameterization . . . . . 3
2.2 Theory . . . . . 5

**3 Sterile effects in cosmology** **6**
3.1 Technical details . . . . . 9
3.2 Results . . . . . 10
3.3 Hints and anomalies: cosmology . . . . . 13

**4 Sterile effects in solar (and KamLAND) neutrinos** **14**
4.1 Technical details . . . . . 14
4.2 Experimental data and fit procedure . . . . . 16
4.3 Results . . . . . 17
4.4 Hints and anomalies: solar data . . . . . 22
4.5 What is the bound on the sterile fraction in solar oscillations? . . . . . 23

**5 Sterile effects in supernovæ and other astrophysical sources of neutrinos** **24**
5.1 Technical details . . . . . 26
5.2 Results . . . . . 29
5.3 Hints and anomalies: supernovæ . . . . . 33
5.4 Neutrinos from other astrophysical sources . . . . . 34

**6 Sterile effects in atmospheric, reactor and beam neutrinos** **35**
6.1 Technical details . . . . . 35
6.2 Results . . . . . 36
6.3 Hints and anomalies . . . . . 39
6.4 LSND . . . . . 39

**7 Summary** **41**

# 1 Introduction

High-energy colliders are the tool to discover new heavy particles with sizable couplings. New light particles with small couplings can be searched for in many different ways. Neutral fermions with eV-scale mass, called 'sterile neutrinos' in the jargon, are typically stable enough to give effects in cosmology, and can affect neutrino oscillation experiments.[1] Both fields recently discovered new physics (in both cases around meV energies), but so far no sterile neutrinos.

Today the most powerful cosmological probe of sterile effects is standard Big-Bang Nucleosynthesis (BBN) [1], which constrains the number of thermalized neutrinos present at $T \sim 0.1\,\mathrm{MeV}$

[1]Small fermions masses are stable under quantum corrections. Cosmology, astrophysics and neutrino experiments are also sensitive to light scalars or vectors, which give different kinds of signals.

to be $N_\nu = 2.5 \pm 0.7$. Since the uncertainty is controversial it is not clear how much $N_\nu = 4$ is disfavoured.

The established solar and atmospheric neutrino anomalies seem produced by oscillations among the three SM neutrinos, with at most minor contributions from possible extra sterile neutrinos. The present 99% C.L. bounds on sterile mixing, computed *assuming* that the initial active neutrino $|\nu_{\rm a}\rangle$ oscillates with a large $\Delta m^2$ into an energy-independent mixed neutrino $\cos\theta_{\rm s}|\nu'_{\rm a}\rangle + \sin\theta_{\rm s}|\nu_{\rm s}\rangle$, are $\sin^2\theta_{\rm s} < 0.25$ in solar oscillations (where $\nu_{\rm a} = \nu_e$) [2] and $\sin^2\theta_{\rm s} < 0.21$ in atmospheric oscillations (where $\nu_{\rm a} = \nu_\mu$) [3].

We relax these simplifying assumptions and study the more general 4-neutrino context. This demands a remarkable effort, but it is an important task for the present, for two reasons. First, because recent discoveries in cosmology and neutrino physics are stimulating new experiments that will study the new phenomena with the redundancy necessary to test the minimal models suggested by present data. Second, because oscillations in extra light particles are the natural extension of the emergent massive neutrinos scenario.

Although we list hints that might be interpreted as sterile neutrino effects (LSND [4], certain pieces of solar or atmospheric or BBN data, ...), we do not focus on any of them in particular. Rather, we compute experimental capabilities and constraints on sterile oscillations and compare them with capabilities and constraints from various present and future cosmological and astrophysical probes. Some important constraints are based on untested assumptions and plagued by systematic uncertainties. In such cases, rather than performing global fits, we identify and compute the key observables, trying to explain the basic physics in simple terms emphasizing the controversial issues, so that the reader can judge.

The paper is organized as follows. In section 2 we briefly review theoretical motivations: as in the case of the known light particles, some fundamental reason would presumably be behind the lightness of an extra sterile neutrino. We also describe the non-standard parametrization of active/sterile mixing that we choose (because more convenient and intuitive than standard parametrizations) and describe the qualitatively different kinds of spectra on which we will focus.

In section 3 we study sterile effects in cosmology, comparing the relative sensitivities of two BBN probes (the helium-4 and deuterium abundances), of Cosmic Microwave Background (CMB) and of Large Scale Structures (LSS). In section 4 we study sterile oscillations in solar (and KamLAND) neutrinos. In section 5 we study sterile oscillations in SN1987A and future supernovæ. We also briefly discuss other less promising probes (relic SN background, high-energy cosmic neutrinos,...). In section 6 we study sterile oscillations in atmospheric and reactor neutrinos, and in short and long-baseline neutrino beams (including LSND).

In order to avoid a unreadably long paper each section is written in a concise way and contains a 'Results' subsection, which can be read skipping the other more technical parts. From a computational point of view, exploring $4\nu$ oscillations is $3 \div 4$ orders of magnitude more demanding than usual 2 or $3\nu$ fits and therefore requires significant improvements of usual techniques. Subsections entitled 'technical details' describe how this was achieved. In particular we describe how we employ the density matrix formalism in neutrino oscillation computations, and explain why even in simple $3\nu$ situations it gives significant advantages with respect to more direct equivalent approaches.

In section 7 we conclude by summarizing and comparing the different probes of sterile neutrinos.

# 2 Active/sterile neutrino mixing

We first introduce a non-standard useful parameterization of the most generic $4\nu$ spectrum, and later present a brief review of theoretical models.

## 2.1 Parameterization

A generic $4 \times 4$ Majorana neutrino mass matrix is described by 4 masses, 6 mixing angles and 6 CP-violating phases; 3 of them affect oscillations.

In absence of sterile neutrinos, we denote by $U$ the usual $3 \times 3$ mixing matrix that relates neutrino flavour eigenstates $\nu_{e,\mu,\tau}$ to active neutrino mass eigenstates $\nu^{\rm a}_{1,2,3}$ as $\nu_\ell = U_{\ell i}\nu^{\rm a}_i$ ($i = \{1,2,3\}$, $\ell = \{e,\mu,\tau\}$). The extra sterile neutrino can mix with one arbitrary combination of active neutrinos,

$$\vec{n}\cdot\vec{\nu} = n_e\nu_e + n_\mu\nu_\mu + n_\tau\nu_\tau = n_1\nu^{\rm a}_1 + n_2\nu^{\rm a}_2 + n_3\nu^{\rm a}_3 \qquad (n_i = U_{\ell i}n_\ell).$$

Mixing of the sterile neutrino can be therefore fully described by a complex unit 3-versor $\vec{n}$ (containing two CP-violating phases) and by one mixing angle $\theta_{\rm s}$. With this parameterization the 4 neutrino mass eigenstates are

$$\begin{cases} \nu_4 = \nu_{\rm s}\ \cos\theta_{\rm s} + n_\ell\nu_\ell\ \sin\theta_{\rm s} \\ \nu_i = U^*_{\ell i}[\delta_{\ell\ell'} - n^*_\ell n_{\ell'}(1-\cos\theta_{\rm s})]\nu_{\ell'} - \sin\theta_{\rm s} n^*_\ell U^*_{\ell i}\nu_{\rm s} \end{cases} \tag{1a}$$

i.e. the $4 \times 4$ neutrino mixing matrix $V$ as that relates flavour to mass eigenstates as $\nu_{e,\mu,\tau,s} = V \cdot \nu_{1,2,3,4}$ is

$$V = \begin{pmatrix} 1-(1-\cos\theta_{\rm s})\vec{n}^*\otimes\vec{n} & \sin\theta_{\rm s}\vec{n}^* \\ -\sin\theta_{\rm s}\vec{n} & \cos\theta_{\rm s} \end{pmatrix} \times \begin{pmatrix} U & 0 \\ 0 & 1 \end{pmatrix} \tag{1b}$$

or, more explicitly,

$$V = \begin{array}{c} \\ \nu_\ell \\ \nu_{\rm s} \end{array} \begin{array}{c} \begin{array}{cc} \nu_i & \nu_4 \end{array} \\ \begin{pmatrix} U_{\ell i} - n_i n^*_\ell(1-\cos\theta_{\rm s}) & n^*_\ell\sin\theta_{\rm s} \\ -n_i\sin\theta_{\rm s} & \cos\theta_{\rm s} \end{pmatrix} \end{array}. \tag{1c}$$

In summary, $\vec{n}$ identifies which combination of active neutrinos mixes with $\nu_{\rm s}$ with mixing angle $\theta_{\rm s}$.

In order to understand how neutrinos oscillate in the generic case, it is convenient to focus on two different kinds of limiting cases, pictorially exemplified in fig. 1:

- **Mixing with a flavour eigenstate** (fig. 1a): $\vec{n}\cdot\vec{\nu} = \nu_\ell$ ($\ell = e$ or $\mu$ or $\tau$). The sterile neutrino oscillates into a well defined flavour at 3 different $\Delta m^2$ (which cannot all be smaller than the observed splittings $\Delta m^2_{\rm sun,atm}$).

- **Mixing with a mass eigenstate** (fig. 1b): $\vec{n}\cdot\vec{\nu} = \nu_i$ ($i = 1$ or 2 or 3).[2] The sterile neutrino oscillates into a neutrino of mixed flavour at a single $\Delta m^2$, which can be arbitrarily small.

[2] From here on, we omit the superscript 'a' (that stands for active): it should be clear that whenever we speak of $\nu_2/\nu_{\rm s}$ mixing, this is just a short-hand for $\nu^{\rm a}_2/\nu_{\rm s}$.

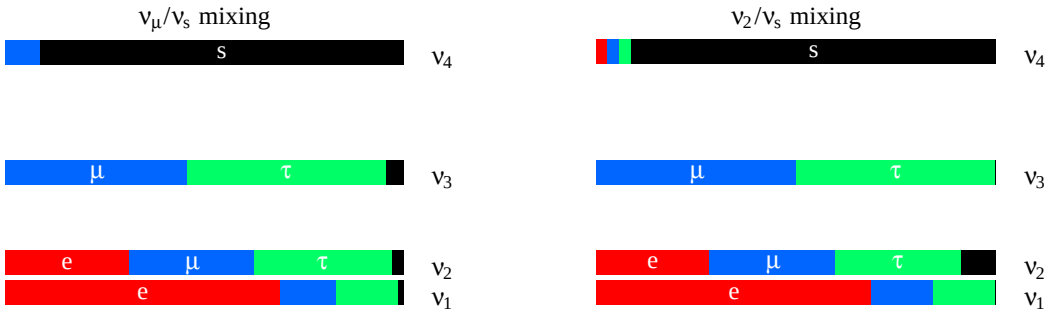


Figure 1: **Basic kinds of four neutrino mass spectra**. *Left: sterile mixing with a flavour eigenstate ($\nu_\mu$ in the picture). Right: sterile mixing with a mass eigenstate ($\nu_2$ in the picture).*

We think that our parametrization of sterile mixing, in eq. (1), makes physics more transparent than other frequently used choices[3].

The oscillation probabilities among active neutrinos in the limit where the active/sterile mass splitting dominates, and active/active mass splittings can be neglected, are

$$P(\nu_\ell \to \nu_{\ell'}) = P(\bar{\nu}_\ell \to \bar{\nu}_{\ell'}) = \begin{cases} 1 - 4|V_{\ell 4}^2|(1 - |V_{\ell 4}^2|)\sin^2(\Delta m_{14}^2 L/4E_\nu) & \text{for } \ell = \ell' \\ 4|V_{\ell 4}^2||V_{\ell' 4}^2|\sin^2(\Delta m_{14}^2 L/4E_\nu) & \text{for } \ell \neq \ell' \end{cases} \quad (2)$$

and in our parametrization $V_{\ell 4} = n_\ell^* \sin\theta_{\rm s}$.

Older papers studied active/sterile mixing in 2 neutrino approximation. In such a case $\theta_{\rm s} = \pi/2$ gives no oscillation effect. On the contrary, in the full 4 neutrino case $\theta_{\rm s} = \pi/2$ swaps the sterile neutrino with one active neutrino. (e.g. $\nu_\mu$ in fig. 1a or $\nu_2$ in fig. 1b, if $\theta_{\rm s}$ were there increased up to $\pi/2$) affecting solar and atmospheric oscillations in an obvious way. Therefore large active/sterile mixing is excluded by experiments for all values of $\Delta m_{i4}^2 \equiv m_4^2 - m_i^2$ (with one exception: the sterile neutrino mixes with a mass eigenstate $\nu_i$ and the two states form a quasi-degenerate pair. This structure arises naturally in certain models [5]).

In order to explore a more interesting slice of parameter space when considering sterile mixing with a mass eigenstate $\nu_i$, for $\theta_{\rm s} > \pi/4$ we modify the spectrum of neutrino masses and replace $(m_i^2, m_4^2)$ with $(2m_i^2 - m_4^2, m_i^2)$. In such a way, the mostly active state always keeps the same squared mass (that we fix to its experimental value), so that in the limit $\theta_{\rm s} = \pi/2$ the sterile neutrino gives no effect rather than giving an already excluded effect. Physically, in our $\nu_{\rm s}/\nu_i$

[3]When studying sterile mixing with a flavour eigenstate our expression is directly related to the 'standard' parameterization

$$V = R_{34}R_{24}R_{14} \cdot U_{23}U_{13}U_{12}$$

where $R_{ij}$ represents a rotation in the $ij$ plane by angle $\theta_{ij}$ and $U_{ij}$ a complex rotation in the $ij$ plane. $\theta_{14}$ or $U_{e4}$ gives rise to $\nu_e/\nu_{\rm s}$ mixing, $\theta_{24}$ or $U_{\mu 4}$ to $\nu_\mu/\nu_{\rm s}$ mixing, and $\theta_{34}$ or $U_{\tau 4}$ to $\nu_\tau/\nu_{\rm s}$ mixing.

The above 'standard' parameterization becomes inconvenient when studying mixing with a mass eigenstate. In such a case our parameterization is directly related to the alternative 'standard' parameterization appropriate for this case,

$$V = U_{23}U_{13}U_{12} \cdot R_{34}R_{24}R_{14}$$

Now $\theta_{i4}$ gives rise to $\nu_i/\nu_{\rm s}$ mixing. Our parameterization instead is convenient because it remains simple in both cases.

plots the mostly sterile neutrino is heavier (lighter) than the mass eigenstate $\nu_i$ to which it mixes when $\theta_{\rm s} < \pi/4$ ($\theta_{\rm s} > \pi/4$). When studying mixing with a flavour eigenstate we do not modify the spectra at $\theta_{\rm s} > \pi/4$ in order to obtain some other experimentally allowed configuration. For this reason, we restrict such plots to $\theta_{\rm s} < \pi/4$.

We do not consider '$2+2$' neutrino mixing, namely two neutrino couples separated by a mass splitting much larger than $\Delta m^2_{\rm sun,atm}$. In fact this spectrum does not reduce to active-only oscillations in any limiting case so that sterile effects are always sizable, and present experiments already exclude this possibility [6]. When the separation among the two couples is comparable to $\Delta m^2_{\rm sun,atm}$, '$2+2$' is no longer a special case qualitatively different from '$3+1$'.

We assume that active neutrinos have normal hierarchy, $\Delta m^2_{23} > 0$. Finally, we assume $\theta_{13} = 0$. We verified that using $\theta_{13} \sim 0.2$, the maximal value allowed by present experiments, leads to minor (in some cases) or no (in other cases) modifications, that we do not discuss. Measuring $\theta_{13}$ and discovering sterile effects will likely be two independent issues (however it is curious to note that both could first manifest as disappearance of reactor $\bar{\nu}_e$).

These assumptions are made because we consider three active neutrinos with normal hierarchy as the most plausible spectrum, and view inverted hierarchy, large $\theta_{13}$ and sterile neutrinos as possible surprises: we here study the latter one.

## 2.2 Theory

The relevant terms in the $\mathrm{SU}(2)_L$-invariant effective Lagrangian that describes active neutrinos $\nu$ together with extra light singlet fermions $\nu_R$ are

$$\frac{m_{LL}}{2v^2}(LH)^2 + \frac{m_{RR}}{2}\nu_R^2 + \frac{m_{LR}}{v}\nu_R LH + \text{h.c.} \tag{3}$$

H is the higgs doublet with vacuum expectation value $(0, v)$. The first dimension-5 operator gives Majorana $\nu$ masses $m_{LL}$ and is naturally small if lepton number is broken at a high-energy scale. The second term gives Majorana $\nu_R$ masses $m_{RR}$, and the third term Dirac $\nu_L\nu_R$ masses $m_{LR}$: one needs to understand why $m_{LR}$ and $m_{RR}$ are small.

A few theoretically favoured patterns emerge from rather general naturalness considerations. We consider the most generic mass matrix with $LL$, $RR$ and $LR$ mass terms. If $m_{LL}$ dominates one obtains light sterile neutrinos with mass $m_{\rm s} \ll m_{\rm a}$ and active/sterile mixings $\theta^2_{\rm s} \sim m_{\rm s}/m_{\rm a}$. If $m_{RR}$ dominates sterile neutrinos are heavy with $\theta^2_{\rm s} \sim m_{\rm a}/m_{\rm s}$. If $m_{LR}$ dominates one obtains quasi-Dirac neutrinos that split into couples. These 'more likely' regions can be represented as lines in the logarithmic $(\tan^2\theta_{\rm s}, \Delta m^2_{i4})$ plane, that we will use to present our results.

A new light particle would probably be a discovery of fundamental importance, because it lightness is likely related to some fundamental principle, as it is the case for the known light particles, the photon, the neutrinos and the graviton. Attempts of guessing physics beyond the SM from first principles motivate a number of fermions which might have $\mathrm{TeV}^2/M_{\rm Pl}$ masses and behave as sterile neutrinos. A few candidates are, in alphabetic order, axino, branino, dilatino, familino, Goldstino, Majorino, modulino, radino. These ambitious approaches so far do not give useful predictions on the flavour parameters in the effective Lagrangian of eq. (3). Therefore one needs to consider more specific ad-hoc models [7].

Unification of matter fermions into SO(10) 16 or $E_6$ 27 representations predicts extra singlets, which however generically receive GUT-scale masses. It is easy to invent ad-hoc discrete

or continuous symmetries that keep a fermion light [7]. One might prefer to use only ingredients already present in the SM. For example, the extra fermions can be forced to be light assuming that they are chiral under some extra gauge symmetry (that could possibly become non perturbative at some QCD-like scale, and give composite sterile neutrinos) [7]. Alternatively, the extra fermions may be light for the same reason why neutrinos are light in the SM [7]. Following this point of view up to its extreme, one can add to the SM a set of 'mirror particles', obtaining 3 sterile neutrinos [7]. In presence of Planck-suppressed corrections that mix the two sectors, mirror neutrinos with the same mass as SM neutrinos give rise to quasi-maximal mixing angles between SM neutrino mass eigenstates and sterile neutrinos, splitted by $\Delta m^2 \sim m_i v^2/M_{\rm Pl} \sim 10^{-8}\,{\rm eV}^2$ (this kind of $\nu_2/\nu_{\rm s}$ effects are disfavoured by solar data). Mirror neutrinos with different masses from SM neutrinos can give detectable $\nu_1/\nu_{\rm s}$ oscillation effects. The two sectors might instead communicate because coupled to the same heavy see-saw neutrinos: this gives massless states which can be mostly sterile.

# 3 Sterile effects in cosmology

Present cosmological data seem compatible with the following minimal assumption (see e.g. [8]): primordial perturbations are generated by minimal inflation (flat space, Gaussian perturbations with flat spectral index $n_s = 1$) and evolve as dictated by general relativity (with a small cosmological constant) and by the Standard Model (adding some unknown Cold Dark Matter). Global analyses performed under this *assumption* give precise determinations of the cosmological parameters and bounds on non standard properties of neutrinos. In particular, the sensitivity to neutrino masses and to oscillations into extra sterile neutrinos is competitive with direct experimental bounds.

Present bounds are unsafe because based on assumptions which have been only partially tested. At the level of precision needed to derive bounds on sterile neutrinos stronger than experimental bounds these assumptions stand practically untested. Since these bounds come from a few key measurements (rather than from a redundant set of different observables) compensations among different kinds of new physics are not unnatural. For instance, the dominant BBN probe [1], the helium-4 abundancy [9], is plagued by controversial systematic uncertainties, and presently it is not clearly incompatible with a fourth thermalized sterile neutrino [10]

Therefore we do not try to attribute a precise probabilistic meaning to cosmological bounds by performing global fits. We prefer to identify and compute the key observables. This allows to present the underlying physics in a simple and critical way (while global fits would indirectly involve other cosmological parameters and data). The implications of present or future measurements can be read from our plots. Cosmology is interesting not only because gives indications today, but also because it will allow powerful future searches.

BBN probes the total energy density at $T \sim (0.1 \div 1)\,{\rm MeV}$ (dominantly stored in electrons, photons and neutrinos according to the SM) and is also directly sensitive to reactions involving neutrinos (e.g. $\bar\nu_e p \leftrightarrow \bar e n$). Given a few input parameters (the effective number $N_\nu$ of thermalized relativistic species, the baryon asymmetry $n_B/n_\gamma = \eta$, and possibly the $\nu_\ell/\bar\nu_\ell$ lepton asymmetries) BBN successfully predicts the abundances of several light nuclei [1]. Its non trivial success strongly indicates that primordial BBN really happened. Today $\eta$ is best determined within minimal cosmology by CMB data to be $\eta = (6.15 \pm 0.25)10^{-10}$ [8]. Thus, neglecting the

lepton asymmetries (which is an excellent approximation unless they are much larger than the baryon asymmetry) one can use the observations of primordial abundances to test if $N_\nu = 3$ as predicted by the SM.

Today the $^4$He abundancy [9] is the most sensitive probe of $N_\nu$. We study also the deuterium abundancy, that might have brighter prospects of future improvements [11]. For arbitrary values of $N_\nu$ around the SM value of 3, BBN predicts [1]

$$Y_p \simeq 0.248 + 0.0096 \ln \frac{\eta}{6.15\ 10^{-10}} + 0.013(N_\nu^{^4\mathrm{He}} - 3), \tag{4a}$$

$$\frac{Y_\mathrm{D}}{Y_\mathrm{H}} \simeq (2.75 \pm 0.13)\ 10^{-5}\ \frac{1 + 0.11\ (N_\nu^\mathrm{D} - 3)}{(\eta/6.15\ 10^{-10})^{1.6}}, \tag{4b}$$

where $Y_p \equiv n_{^4\mathrm{He}}/n_B$. Both $Y_p$ and $Y_\mathrm{D}$ are plagued by controversial systematic uncertainties. We do not enter into these issues and refer the reader to [12, 13, 10, 9, 11]. Adopting conservative estimates we get

$$\begin{array}{lll} Y_p = 0.24 \pm 0.01 & \Rightarrow & N_\nu^{^4\mathrm{He}} \simeq 2.4 \pm 0.7, \\ \dfrac{Y_\mathrm{D}}{Y_\mathrm{H}} = (2.8 \pm 0.5)\, 10^{-5} & \Rightarrow & N_\nu^\mathrm{D} \simeq 3 \pm 2. \end{array} \tag{5}$$

In order to safely test and possibly rule out $N_\nu = 4$ it is necessary to either *i*) somewhat improve the determination of $Y_p$, or to *ii*) improve on $Y_\mathrm{D}$, somewhat improve on $\eta$ and on the theoretical uncertainty on $Y_\mathrm{D}$.

In our computation, we assume standard cosmology plus a sterile neutrino, and conservatively assume it has zero initial abundancy at $T \gg$ MeV. Oscillations produce sterile neutrinos [14]. This is a rather robust phenomenon: it is difficult to modify cosmology in order to avoid production of sterile neutrinos while keeping the success of BBN. In fact sterile neutrinos are dominantly produced at $T \sim$ MeV, simultaneously or after neutrino decoupling.

However, a neutrino asymmetry $\eta_\nu$ 8 orders of magnitude larger than $\eta$ in baryons is a significant extra parameter: it affects the $\nu_e$ abundancy and consequently the $n/p$ ratio at freeze-out, and finally the primordial abundances. Also, a relatively large lepton asymmetry, around $10^{-5}$, gives extra MSW effects which can suppress active/sterile oscillations removing cosmological signals [15]. More generically, allowing a non vanishing $\eta_\nu$ any $N_\nu$ is compatible with the measurement of the helium-4 abundancy, just because a single measurement cannot fix two parameters ($N_\nu$ and $\eta_\nu$). It is important to study how the situation improves when also $Y_\mathrm{D}$ will be precisely measured. For example increasing $N_\nu$ from 3 to 4 increases $Y_\mathrm{D}$ by 11% and $Y_p$ by 5%. If the latter effect were compensated by a large neutrino asymmetry, $Y_\mathrm{D}$ still remains about 8% higher. Numbers can be somewhat different, depending on how $N_\nu$ gets dynamically increased by sterile oscillations, which are also directly affected by a large neutrino asymmetry in an important way [15, 16]. However the general point remains. Of course one can make any $N_\nu$ allowed by just introducing more than one free parameter; but measuring two or more observables would make hard to believe that new physics effects cancel among each other in all cases.

In the following we stick to standard cosmology.

For each choice of oscillation parameters, we follow the evolution with temperature of neutrino abundances and compute how $Y_p$ and $Y_\mathrm{D}$ are modified. For easy of presentation, we convert their values into effective numbers of neutrinos, $N_\nu^{^4\mathrm{He}}$ and $N_\nu^\mathrm{D}$, univocally defined by the inversion of

eq. (4). These parameters do not necessarily lie between 3 and 4 and are employed just as a useful way of presenting our final results.

We also compute another effective number of neutrinos, that parameterizes the total energy density in relativistic species at photon decoupling as[4]

$$\rho_{\rm relativistic} = \rho_\gamma \Big[1 + \frac{7}{8}\Big(\frac{4}{11}\Big)^{4/3} N_\nu^{\rm CMB}\Big]. \tag{6}$$

This quantity (together with other cosmological parameters) determines the pattern of fluctuations of the CMB measured by WMAP (and other experiments). Neutrinos affect CMB in various ways [17]; in the future studying how neutrino free-streaming shifts the acoustic peaks should offer a clean way of directly counting neutrinos. Global fits at the moment imply [18]

$$N_\nu^{\rm CMB} \approx 3 \pm 2 \tag{7}$$

somewhat depending on which priors and on which data are included in the fit. Future data might start discriminating 3 from 4 neutrinos.

Finally, neutrinos can be studied looking at distribution of galaxies because massive neutrinos move without interacting, making galaxies less clustered [19]. The effect depends on two parameters, that in absence of sterile neutrinos are both determined by neutrino masses: 1) the temperature at which neutrinos become non relativistic, $T_\nu \sim m_\nu/3$ (so that active neutrinos operated when the horizon of the universe had the size that clusters of galaxies have now); 2) the energy density in neutrinos, $\Omega_\nu h^2$, that determines how large is the effect of neutrinos (neutrinos give at most a minor correction). As usual, the parameter $h$ is $H_{\rm today}/(100{\rm km/s\,Mpc})$.

Global analyses of cosmological data are usually reported as a bound on $\Omega_\nu$, assuming the standard correlation with $T_\nu$ [8, 19]. However, in presence of a non-thermal population of sterile neutrinos these two parameters are no longer universally related. E.g. there could be a little number of sterile neutrinos with few eV mass (heavy neutrinos affect also CMB, behaving as cold dark matter). This scenario has not yet been compared with present data (see [20] for closely related work). We assume that the bound can be approximated with the standard one on the following quantity:[5]

$$\Omega_\nu h^2 = \frac{{\rm Tr}[m \cdot \rho]}{93.5\,{\rm eV}} \tag{8}$$

where $m$ is the $4 \times 4$ neutrino mass matrix and $\rho$ is the $4 \times 4$ neutrino density matrix, as discussed below. We approximate the present bound with $\Omega_\nu h^2 < 0.01$ (e.g. the WMAP global fit gives $\Omega_\nu h^2 < 0.76\ 10^{-2}$ at 95% C.L. in the standard case [8]. The bound becomes slightly weaker if $N_\nu^{\rm CMB} = 4$, or if more conservative priors or estimates of systematic uncertainties are adopted [19]). The atmospheric mass splitting guarantees $\Omega_\nu \gtrsim 0.5\ 10^{-3}$ so that future attempts to reach this level of sensitivity are guaranteed. We assume that a 0.001 sensitivity in $\Omega_\nu h^2$ will be reached.

[4] Including small effects of spectral distortions the precise SM prediction for the effective number of neutrinos is $N_\nu^{\rm CMB} = 3.04$, but we can ignore this subtlety.

[5] We are neglecting CP-violation, and assuming that neutrinos and anti-neutrinos have equal density matrices.

### 3.1 Technical details

Before discussing results, we present the main technical details. In order to compute the observables discussed above one needs to set up the network of relevant Boltzmann equations and study neutrino oscillations in the early universe [21, 22]. We use our BBN code that includes all main effects, relying on more accurate public codes only to precisely fix the central SM values. This is a complicated computation because many processes proceed at $T \sim$ MeV: active (and maybe sterile) neutrino oscillations, neutrino decoupling, neutron decay, electron decoupling and finally nucleosynthesis. The various processes have been accurately studied in the past. The extension from 2 neutrinos oscillations to 4 neutrinos oscillations does not involve new ingredients, but rewriting and implementing old ones in an appropriate way is not completely trivial due to the presence e.g. of oscillations at different frequencies.

Brute force alone would not allow to explore the key observables in a vast parameter space: it is necessary to employ accurate approximations that one can invent understanding the physics of BBN. Neglecting spectral distortions possibly induced by active/sterile oscillations, the Boltzmann equation for the $4 \times 4$ neutrino (and anti-neutrino) density matrix is [21, 22]

$$\dot{\rho} = zZH\frac{d\rho}{dz} = i[\mathscr{H},\ \rho] - \{\Gamma, (\rho - \rho^{\rm eq})\}. \tag{9}$$

where $H$ is the Hubble constant at temperature $T$, $z = m_e/T$. The factor $Z = -3\ {\rm d}\ln z/{\rm d}\ln s$ (where $s$ is the entropy density) differs from 1 when the temperature of the universe does not decrease as the inverse of its comoving radius, namely during electron decoupling ($z \sim 1$) and when sterile neutrinos thermalize. In the flavour basis [21]

$$\mathscr{H} = \frac{mm^\dagger}{2E_\nu} - \frac{7\pi^3\, T_\nu\, \alpha_2}{15\, M_W^4}\Big[T_\nu^4 \cos^2\theta_{\rm W}\ {\rm diag}\,(\rho_{ee}, \rho_{\mu\mu}, \rho_{\tau\tau}, 0) + 2\ T^4\ {\rm diag}\,(1,0,0,0)\Big] \tag{10}$$

We can neglect contributions from the off-diagonal elements of $\rho$ [21]. The usual MSW effect [23] gives an additional subdominant term with different sign for neutrinos and antineutrinos. The average over the neutrino energy spectra is performed using a Fermi-Dirac distributions, and therefore neglecting spectral distortions possibly caused by oscillations.

In eq. (9) we use the standard 'anticommutator' approximation for the collision terms $\Gamma$, that describe weak $\nu e$ and $\nu\nu$ interactions that tend to thermalize neutrinos, driving their matrix density to its thermal equilibrium value, $\rho^{\rm eq} = {\rm diag}(1,1,1,0)$. A detailed comparison with the full equations [22] reveals that they are accurately mimicked by inserting the following values of the damping coefficients. In the equations for the off-diagonal components of $\rho$, we insert the total scattering rate [22]

$$\Gamma_{\rm tot} \approx 3.6\ G_{\rm F}^2\ T^5 \quad \text{for } \nu_e \qquad \text{and} \qquad \Gamma_{\rm tot} \approx 2.5\ G_{\rm F}^2\ T^5 \quad \text{for } \nu_{\mu,\tau}$$

because all scatterings damp the coherent interference between different flavours. In the equations for the diagonal components of $\rho_{ii}$, we insert the annihilation rate [22]

$$\Gamma_{\rm ann} \approx 0.5\ G_{\rm F}^2\ T^5 \quad \text{for } \nu_e \qquad \text{and} \qquad \Gamma_{\rm ann} \approx 0.3\ G_{\rm F}^2\ T^5 \quad \text{for } \nu_{\mu,\tau}$$

since annihilations are needed to change the number of neutrinos. However this procedure [22] introduces an artificial choice of basis, giving equations which are no longer invariant under

rotations in the $(\mu, \tau)$ sector. In order to correctly maintain important coherencies among $\nu_\mu$ and $\nu_\tau$, we introduce the distinction between $\Gamma_{\rm tot}$ and $\Gamma_{\rm ann}$ in the $\nu_\mu \pm \nu_\tau$ basis (assuming maximal atmospheric mixing; otherwise the generalization is immediate).

After determining neutrino evolution we can study the relative $n/p$ abundancy, that evolves according to [1, 14]

$$\dot{r} = zHZ\frac{dr}{dz} = \Gamma_{p\to n}(1-r) - r\Gamma_{n\to p} \qquad r = \frac{n_n}{n_n + n_p}$$

where $\Gamma_{p\to n}$ is the total $pe\bar{\nu}_e \to n$, $pe \to n\nu_e$ and $p\bar{\nu}_e \to n\bar{e}$ reaction rate (in thermal equilibrium the inverse process would satisfy $\Gamma_{n\to p} = \Gamma_{p\to n} e^{(m_n - m_p - m_e)/T}$). The production of sterile neutrinos affects $n/p$ by [14] 1) increasing the Hubble parameter $H$; 2) modifying the $\Gamma_{p\to n}, \Gamma_{n\to p}$ rates, if the $\nu_e$ population is depleted by oscillations.

Finally a network of Boltzmann equations describes how electroweak, strong and electromagnetic processes control the evolution of the various nuclei: $p$, $n$, D, T, $^3$He, $^4$He,... Rather than recalling here the main features of these equations, we just state (without explanation) the approximation we use (see also [24]). At a sufficiently low temperature $T^* \sim 0.08\,\mathrm{MeV}$ almost all neutrons wind up in $^4$He, so that its mass abundancy is given by $Y_p \simeq 2r(T^*)$ with $T^*$ obtained solving

$$180H = \Gamma_{\rm DD\to pT}(\Gamma_{pn\to {\rm D}\gamma}/\Gamma_{{\rm D}\gamma\to pn})^2.$$

The precise numerical value is fixed in such a way that in the SM case our simplified code precisely agrees with state of the art codes (that include thermal, radiative and other corrections corrections, smaller than the present experimental uncertainty).[6] The deuterium abundancy is obtained with a similar technique.

## 3.2 Results

We plot the effective numbers $N_\nu$ of neutrinos defined in terms of the physical observables (the $^4$He and D abundances and the energy density at recombination) from eq.s (4) and (6). We also plot the value of the present energy density in neutrinos $\Omega_\nu$, probed by observations of Large Scale Structure together with CMB constraints.

The plots have the following meaning: shaded regions have $N_\nu^{^4{\rm He}} > 3.8$ or $\Omega_\nu h^2 > 10^{-2}$ and are therefore 'disfavoured' or 'excluded' (depending on how conservatively one estimates systematic uncertainties) within minimal cosmology. The other lines indicate the sensitivity that future experiments might reach. More precisely we plot contour-lines corresponding to $N_\nu = 3.2$ and 3.8 and to $\Omega_\nu h^2 = 10^{-2}$ and $10^{-3}$.

[6] A recent paper [25] studied, in a four-neutrino context, how active/sterile oscillations affect the $^4$He abundancy. The authors of [25] take into account spectral distortions of $\nu_{\rm s}$ (that we neglect), and neglects other minor corrections (that we include), such as those related to the electron mass. They compute an 'effective BBN neutrino number' $N_\nu^{\rm BBN}$, which, unlike our $N_\nu^{^4{\rm He}}$ and $N_\nu^{\rm D}$, is not directly related to the observable helium-4 and deuterium abundances. However, in the parameter range covered by their plots, their $N_\nu^{\rm BBN}$ should be an approximation to $N_\nu^{^4{\rm He}}$. The plots that can be compared show a reasonable level of agreement.

At $\Delta m^2 \sim 10^{-8}\,\mathrm{eV}^2$ spectral distortions of electron neutrinos are not negligible: in the two-neutrino limit they make the helium-4 abundancy more sensitive to sterile oscillations (see the papers by Kirilova et al. in [16]).

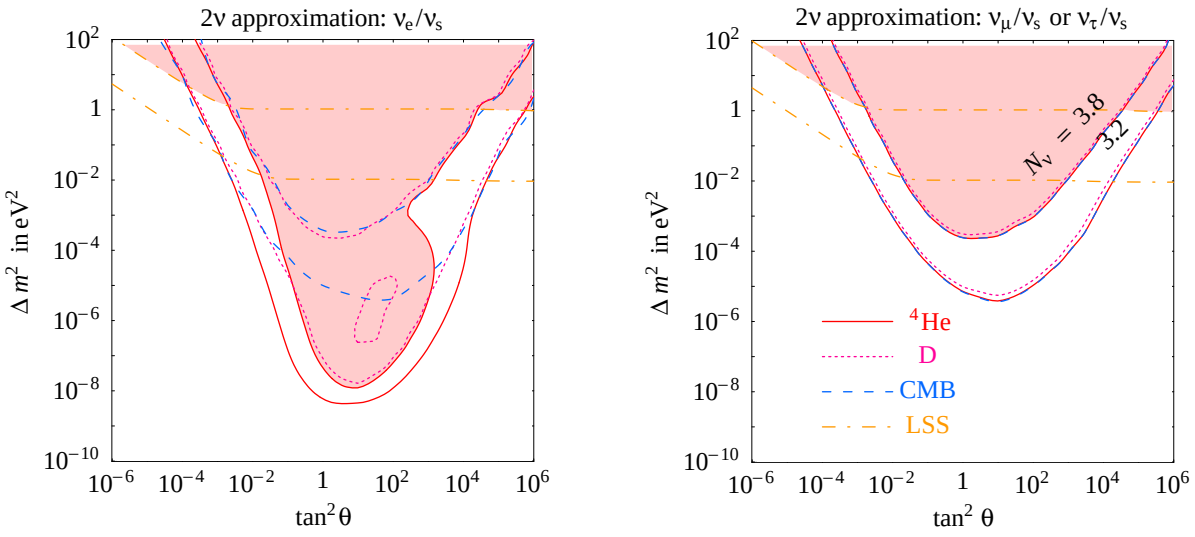


Figure 2: *Isocurves to the effective number of neutrinos produced by 2 neutrino oscillations in the cases $\nu_e/\nu_s$ (left plot) and $\nu_{\mu,\tau}/\nu_s$. Solar and atmospheric oscillations are included in the 3 neutrino plots of fig. 3, where the meaning of the various isolines is precisely explained.*

It is useful to start discussing the unrealistic but simple cases considered in old papers [14]. In fig. 2 we show the effects produced by 2 neutrino mixing: $\nu_s/\nu_e$ in fig. 2a and $\nu_s/\nu_\mu$ or $\nu_s/\nu_\tau$ mixing in fig. 2b.[7] The red dashed line shows the total number of neutrinos, $N_\nu^{\rm CMB}$: it essentially does not depend on which flavour ($\nu_e$, $\nu_\mu$ or $\nu_\tau$) mixes with $\nu_s$ and is not affected by oscillations with $\Delta m^2 \lesssim 10^{-5}\,{\rm eV}^2$ that are too slow and start only after neutrino decoupling, when the total number of neutrinos is frozen.[8] At this stage neutrinos can still change flavour. The difference between fig. 2a and 2b is due to the fact that only electron neutrinos are involved in the reactions that control the $n/p$ ratio. Therefore $\nu_s/\nu_e$ oscillations that occur after neutrino freeze-out and that do not affect the total number of neutrinos ($\nu_s$ are created by depleting $\nu_e$) affect $n/p$ and consequently the $^4$He abundancy[9] (continuous line) [14] and, to a lesser extent, the D abundancy. This happens down to $\Delta m^2 \sim 10^{-8}\,{\rm eV}^2$: oscillations with $\Delta m^2 \lesssim 10^{-8}\,{\rm eV}^2$ occur after decoupling of electroweak scatterings, when the relative $n/p$ abundancy is only affected by neutron decay.

Effects are larger at $\theta > \pi/4$ (i.e. $\tan\theta > 1$) because this corresponds to having a mostly sterile state lighter than the mostly active state, giving rise to MSW resonances in neutrinos and anti-neutrinos (like in cosmology, also supernova $\bar\nu_e$ feel a MSW resonance for $\theta_s \gtrsim \pi/4$.

[7] Previous papers studied the $^4$He abundancy and we agree with their results. We however use as a variable $\tan^2\theta$ rather than $\sin^2 2\theta$, so that we unify in a unique plot the non-resonant ($0 < \theta < \pi/4$) and the resonant ($\pi/4 < \theta < \pi/2$) case.

[8] To be precise we should say 'the total entropy in neutrinos per comoving volume remains constant'. For simplicity we will adopt such loose abbreviations.

[9] These region are strongly disfavoured because have a helium-4 abundancy corresponding to $N_\nu^{^4{\rm He}} > 4$, up to about 5.

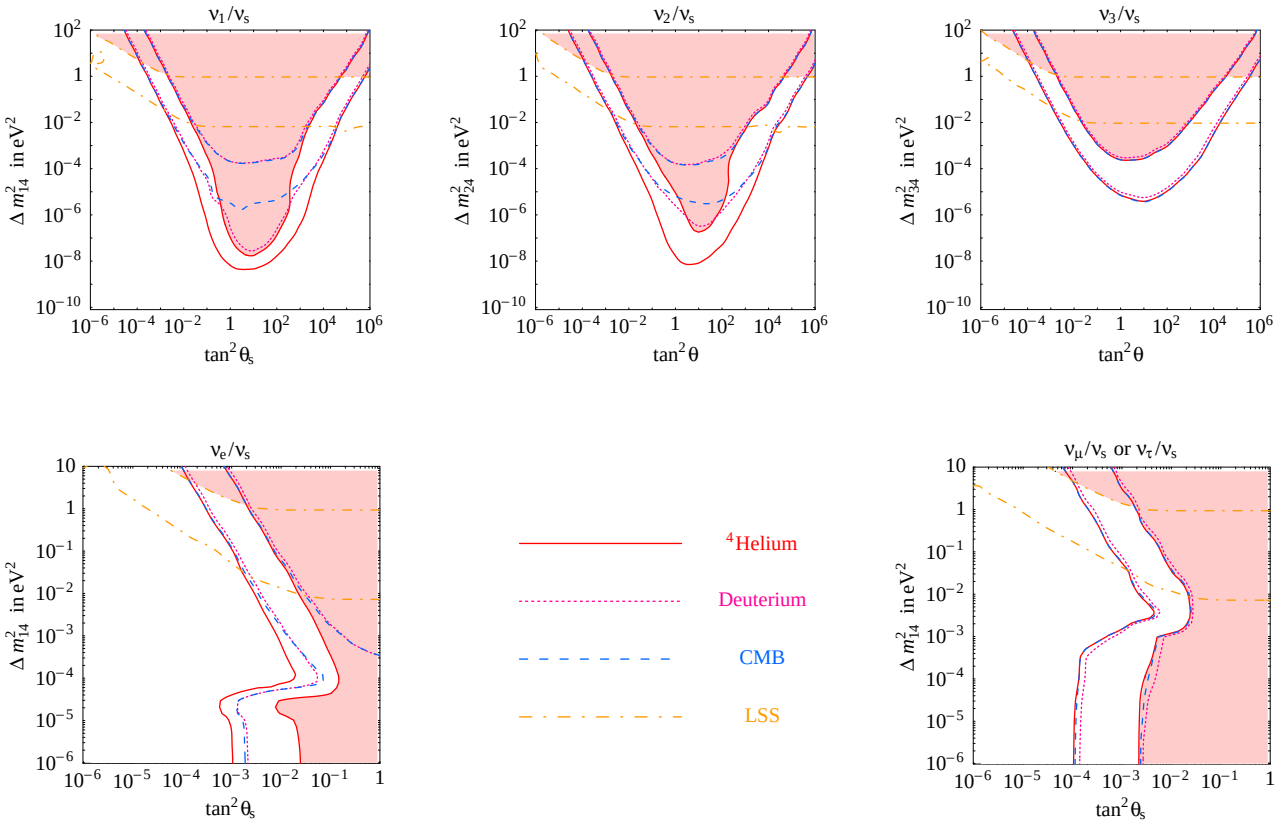


Figure 3: **Cosmological effects of sterile neutrino oscillations**. *We compare four different signals. The continuous red line refers to the* $^4$He *abundancy (we shaded as 'disfavoured' regions where its value corresponds to* $N_\nu > 3.8$*), the violet dotted line to the deuterium abundancy, and the dashed blue line to the effective number of neutrinos at recombination. We plotted isolines of these three signals corresponding to an effective number of neutrinos* $N_\nu = 3.2$ *and* $3.8$*. The precise meaning of the parameter* $N_\nu$ *in the three cases is explained in the text. The upper (lower) dot-dashed orange lines corresponds to* $\Omega_\nu h^2 = 10^{-2}$ $(10^{-3})$*, where* $\Omega_\nu$ *is the present energy density in neutrinos.*

On the contrary solar neutrinos feel a resonance for $\theta_s \lesssim \pi/4$). In the past years it has been debated about if a neutrino asymmetry and/or large inhomogeneity develop as a consequence of non-linear effects, and this issue has not yet been fully clarified. Our Boltzmann equations assume that both these effects can be neglected. At $\tan\theta > 1$ the bound from $\Omega_\nu$ holds even for very small mixing, $\theta \simeq \pi/2$ just because these region correspond to heavy active neutrinos.

We now discuss how the above picture changes taking into account oscillations among active neutrinos. Our results are shown in fig. 3: the upper row refers to sterile mixing with mass eigenstates $\nu_{1,2,3}$ and the lower row to mixing with flavour eigenstates $\nu_e$ and $\nu_{\mu,\tau}$.

An inspection of the upper row shows that their main features can be understood in terms of the (unrealistic) results in the case of 2 neutrino mixing, fig. 2. Having assumed $\theta_{13} = 0$, $4\nu$ sterile mixing with $\nu_3$ gives no new effects with respect to $2\nu$ sterile mixing with $\nu_{\mu,\tau}$. Due to solar and atmospheric oscillations, $\nu_e$ depletion due to oscillations into sterile neutrinos now happens in all other cases and becomes milder, because no longer confined to $\nu_e$ but shared among all active neutrinos. Fig. 3b shows the effects of $\nu_s/\nu_2$ mixing (this kind of neutrino spectrum is plotted in fig. 1b): since $\nu_2$ contains some $\nu_e$ component, electron neutrinos are in part directly affected. Fig. 3a shows the effects of $\nu_s/\nu_1$ mixing: $\nu_e$ depletion effects are largest in this last case because $\nu_1$ is the neutrino eigenstate with the largest $\nu_e$ component. In summary: depletion gets transferred to all $\nu$ flavours and diluted.

Mixing with flavour eigenstates is qualitatively different, for the general reasons explained in section 2. We can see the effects of the solar (atmospheric) mass splitting as bumps in fig. 3d (3e) where cosmological effects of $\nu_s/\nu_e$ ($\nu_s/\nu_{\mu,\tau}$) mixing are computed. In the case of $\nu_s/\nu_e$ mixing $N_\nu^{\rm D}, N_\nu^{\rm CMB} = 4$ is reached only if the sterile neutrino has a large enough $\Delta m^2$: the solar $\Delta m^2_{\rm sun} \approx 0.7\ 10^{-4}\,{\rm eV}^2$ alone is not sufficient, as also indicated by the $2\nu$ limit plotted in fig. 2a. On the contrary, fig. 2b shows that in the case of $\nu_s/\nu_{\mu,\tau}$ mixing a $\Delta m^2 \sim \Delta m^2_{\rm atm} \approx 2\ 10^{-3}\,{\rm eV}^2$ is large enough to reach $N_\nu \approx 4$ for any value of the sterile mass. We have verified that setting $\theta_{13} \sim 0.2$ fig.s 3 do not vary in a significant way.

### 3.3 Hints and anomalies: cosmology

To conclude we list cosmological data that do not fit well into the scheme presently considered as standard, and that can be interpreted as manifestations of sterile neutrino effects:

- Various determinations of the primordial helium-4 abundancy $Y_p$ try to reduce uncertainties by appropriately choosing and modeling the astrophysical systems used for the observation [9]. Some analyses find lower values of $Y_p$ corresponding to less than 3 neutrinos (an effect which could come from active-sterile oscillations), even after a detailed examination of the systematic uncertainties. Other determinations give higher values of $Y_p$, more compatible with $N_\nu = 3$.

- $X$-ray cluster data seem to prefer a lower value of the parameter $\sigma_8$ than the other sets of CMB and LSS data, considered in [8, 19]. A degenerate spectrum of active neutrinos can alleviate this discrepancy [26]. Otherwise, one can invoke a contribution to $\Omega_\nu$ from sterile neutrinos.

- Decays of sterile neutrinos with mass $\sim 200\,\mathrm{MeV}$ provide an interpretation of the reionization at large redshift observed by WMAP, alternative to the standard one (early formation of massive stars) [27].
- Decays of sterile neutrinos with mass $\sim 10\,\mathrm{MeV}$ and abundancy $\Omega_\nu = 10^{-5\div 9}$ can be a non standard source of recently observed galactic positrons [28].

# 4 Sterile effects in solar (and KamLAND) neutrinos

We compare sterile effects with present and future solar neutrino experiments and with KamLAND reactor anti-neutrino data. While computing sterile effects in reactor $\bar{\nu}_e$ is straightforward, solar neutrinos are detected after a long trip from the center of the sun during which they can experience sterile effects in several different ways. This is what makes solar neutrinos a powerful probe of sterile effects. In section 4.1 we describe how we precisely compute these effects. Section 4.2 describes how we fit data, dealing with the complication that these data contain a positive evidence for active/active oscillations. Results and a qualitative understanding are presented in section 4.3. In section 4.5 we compare our results with previous analyses performed in limiting cases.

## 4.1 Technical details

In order to understand what happens when a sterile neutrino is added and to write a sufficiently fast numerical code, we must develop an analytical approximation. It is convenient to employ some more formalism than in the $2 \times 2$ case and study the evolution of the $4 \times 4$ neutrino density matrix $\rho_m$ written in the $m$ass basis of instantaneous mass eigenstates. A $\nu_e$ produced with energy $E_\nu$ at radius $r = r_0$ inside the sun is described by $\rho_m = V_m^\dagger \cdot \mathrm{diag}\,(1,0,0,0) \cdot V_m$ where $V_m$ depends on $E_\nu$ and $r_0$. Mixing matrices in matter ($V_m$) and vacuum ($V$) are computed diagonalizing the Hamiltonian [23]

$$\mathscr{H} = \frac{mm^\dagger}{2E_\nu} + \sqrt{2} G_{\mathrm{F}} \mathrm{diag}\,(N_e - \frac{N_n}{2}, -\frac{N_n}{2}, -\frac{N_n}{2}, 0)$$

and ordering eigenstates according to their eigenvalues $H_i \equiv m^2_{\nu_{mi}}/2E_\nu$: $\nu_{m1}$ ($\nu_{m4}$) is the lightest (heaviest) neutrino mass eigenstate in matter. The evolution up to the detection point is described by a $4\times4$ unitary evolution matrix $\mathscr{U}$ so that at detection point the density matrix in the basis of flavour eigenstates is $\rho = \langle V \cdot \mathscr{U} \cdot \rho_m(r, E_\nu) \cdot \mathscr{U}^\dagger \cdot V^\dagger \rangle$. where $\langle \cdots \rangle$ denotes average over the production point. The various observables involve additional averages over neutrino energy and time (and consequently over different paths in the earth and in vacuum). The oscillation probabilities are given by $P(\nu_e \to \nu_e) = \rho_{ee}$, $P(\nu_e \to \nu_{\mathrm{s}}) = \rho_{ss}$, etc.

We briefly describe the main steps in the computation of $\mathscr{U}$, focussing on the subtle ones. The evolution matrix can be decomposed as

$$\mathscr{U} = \mathscr{U}_{\mathrm{earth}} \cdot \mathscr{U}_{\mathrm{vacuum}} \cdot \mathscr{U}_{\mathrm{sun}}.$$

Evolution in vacuum is given by $\mathscr{U}_{\mathrm{vacuum}} = \mathrm{diag}\,\exp(-iLm^2_{\nu_i}/2E_\nu)$. Combined with average over neutrino energy it suppresses the off-diagonal element $\rho^{ij}_m$ when the phase differences among eigenstates $i$ and $j$ are large.

Evolution in the earth is computed in mantle/core approximation, improved by using the average density appropriate for each trajectory as predicted in [29]. Therefore we use $\mathscr{U}_{\rm earth} = 1$ when the earth is not crossed, $\mathscr{U}_{\rm earth} = P \cdot {\rm diag}\,\exp(-iL_{\rm mantle} m^2_{\nu_{mi}}/2E_\nu) \cdot P^\dagger$ when only the mantle is crossed (for a length $L_{\rm mantle}$), and the obvious generalization when both mantle and core are crossed. $P = V_B^\dagger V_A$ is a non-adiabaticity factor that takes into account the sharp flavour variation of mass eigenstates when passing from medium $A$ (vacuum) into medium $B$ (the earth mantle) .

Evolution in the sun is more complicated because there can be various $P$ factors at non-adiabatic level crossings at radii $r_n$ ($n = 1, 2, \ldots, n_{\rm max}$), that give

$$\mathscr{U}_{\rm sun} = P_{r_n} \cdots P_{r_2} \cdot {\rm diag}\,\exp(-i \int_{r_1}^{r_2} ds\ \frac{m^2_{\nu_{mi}}}{2E_\nu}) \cdot P_{r_1} \cdot {\rm diag}\,\exp(-i \int_{r_0}^{r_1} ds\ \frac{m^2_{\nu_{mi}}}{2E_\nu})$$

The number of level crossings $n_{\rm max}$ ranges between 0 and a few, e.g. a $\nu_e$ produced in the side of the sun farther from us can experience 4 crossings. When levels $i$ and $j$ cross in an adiabatic way, $P_{r_n} = 1$. If instead level crossing is fully non adiabatic $P_{r_n} = V_m^\dagger(r \lesssim r_n) \cdot V_m(r \gtrsim r_n)$ is a rotation with angle $\alpha = 90^\circ$ in the $(ij)$ plane. In general the rotation angle is given by $\tan^2\alpha = P_C/(1 - P_C)$, where $P_C$ is the level crossing probability.

So far we only presented the well known formalism [23, 30, 31] in a non standard way appropriate for applying it in numerical computations with multiple and overlapping level crossings. We now need to compute $P_C$. This last step turns out to be non trivial. By generalizing well known results valid in the simpler $2 \times 2$ case [30, 31], we find that in all the parameter range $P_C$ can be accurately approximated analytically (i.e. no need of numerically solving the differential neutrino evolution equation $i\, d\rho/ds = [\mathscr{H}, \rho]$). Such a simple result is possible because, in the relevant neutrino energy range, level crossings are non adiabatic only for $\theta_{\rm s}^2 \cdot \Delta m^2/10^{-8}\,{\rm eV}^2 \gg 1$ i.e. when either $\theta$ is small or the active/sterile $\Delta m^2$ is much smaller than the LMA splitting.

To compute $P_C$ it is convenient to consider the basis of mass eigenstates in absence of active/sterile mixing (i.e. $\theta_{\rm s} \to 0$ or $\theta_{\rm s} \to \pi/2$, depending on which limit is closer to the value of $\theta_{\rm s}$ under examination. Here we focus on $\theta_{\rm s} \to 0$.). This limit allows to precisely define level-crossings. When $\nu_{\rm s}$ crosses one of the active eigenstates, $\nu_a^m$ ($a = 1, 2, 3$) (see fig. 1a for one example), the level crossing probability $P_C$ is well approximated by

$$P_C = \frac{e^{\tilde\gamma \cos^2\theta^m_{as}} - 1}{e^{\tilde\gamma} - 1} \qquad \gamma = \frac{4\mathscr{H}^2_{as}}{dH_a/dr} \equiv \tilde\gamma \cdot \frac{\sin^2 2\theta^m_{as}}{2\pi|\cos 2\theta^m_{as}|} \quad \text{where} \quad \sin\theta^m_{as} = \vec n \cdot \vec\nu^m_a \sin\theta_{\rm s}. \qquad (11)$$

The above equation might seem a complicated way of rewriting the well known expression for $P_C$ valid in the simpler $2\nu$ case [30, 31], but there is one important difference. In the $2\nu$ case one can write the result in an analogous way, which contains the mixing angle in vacuum and the off-diagonal elements of the Hamiltonian in vacuum. On the contrary, our $\gamma$ and $\theta^m_{as}$ must be computed around the resonance, where $\mathscr{H}_{aa} = \mathscr{H}_{ss}$ (or around the point where adiabaticity is maximally violated, in cases where there is no resonance). We emphasize that reducing the full $4 \times 4$ Hamiltonian to the effective $2 \times 2$ Hamiltonian of the 2 states that cross and computing $\mathscr{H}_{as}$ is non trivial, since sterile mixing sometimes redefines the flavour of the active neutrino involved in the crossing.[10] In these situations it is useful to know the physical meaning of $2\mathscr{H}_{as}$: it is the

[10] Neglecting this subtlety would give a qualitatively wrong result e.g. in the following situation: $\nu_{\rm s}$ is mixed with $\nu_e$ and is quasi degenerate to $\nu_1$.

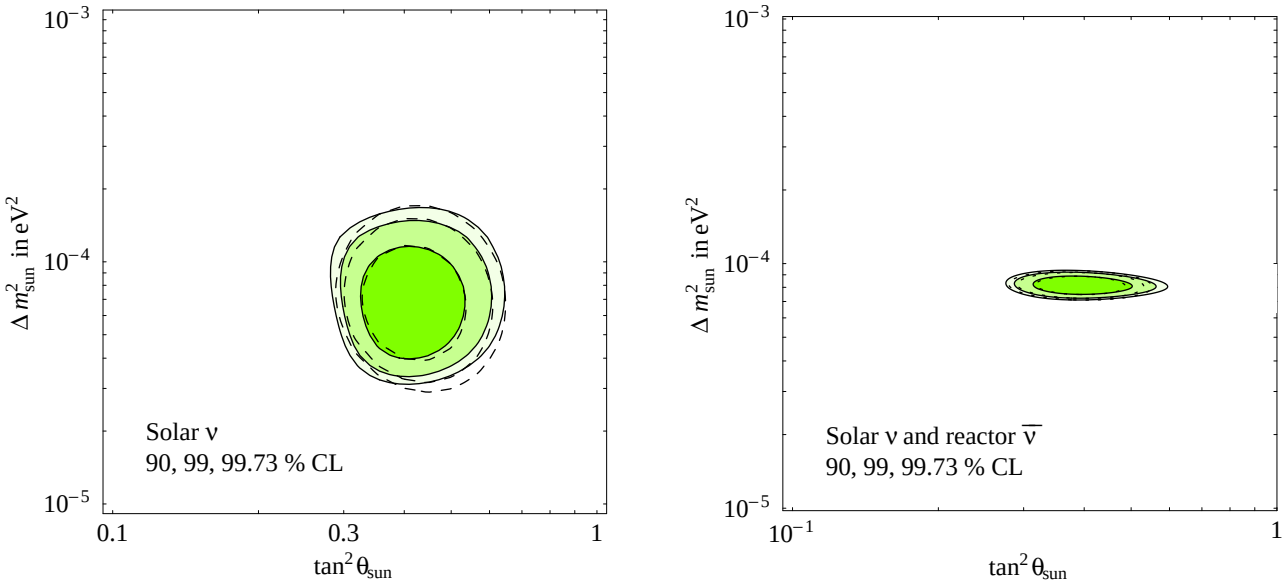


Figure 4: *We compare the usual 'active only' global fit of solar (shaded regions in the left plot) and of solar plus KamLAND data (shaded regions in the right plot), with the Gaussian approximation employed in this paper (dashed lines)*

minimal difference between the eigenvalues of the two states that cross. In order to elucidate the physical meaning of the crossing angle $\theta^m_{as}$, we emphasize that it can also be extracted from the scalar product between the flavour vectors of the two matter eigenstates $i$ and $i+1$ that cross: $\sin\theta^m_{as} = \nu^*_{m_i}(r \lesssim r_n) \cdot \nu_{m_i}(r \gtrsim r_n)$ and $\cos\theta^m_{as} = \nu^*_{m_i}(r \lesssim r_n) \cdot \nu_{m_{i+1}}(r \gtrsim r_n)$.

When the active/sterile mixing is large, $P_C$ is sizable only if $\Delta m^2_{as} \ll \Delta m^2_{\rm LMA}$: in this case our expression (11) reduces to the standard 2-neutrino formula. In the narrow resonance limit (e.g. for $\theta^m_{as} \ll 1$), eq. (11) reduces to a Landau-Zener form $P_C \simeq e^{-\pi\gamma/2}$: our expression for the adiabaticity factor $\gamma$ holds for a generic $2\times 2$ Hamiltonian. In the sun, resonances with $\theta^m_{as}$ close to $\pi/4$ happen only in the quasi-vacuum region at the border of the sun. This will be no longer true when studying supernova neutrinos, that will necessitate an extension of eq. (11).

## 4.2 Experimental data and fit procedure

We fit all available latest data:

- The SNO CC+NC+ES spectra [32], divided in 34 bins (17 energy bins times 2 day/night bins).
- The total CC, NC and ES rates measured by SNO with enhanced NC sensitivity [33].
- The Super-Kamiokande ES spectra [34], divided in 44 zenith-angle and energy bins.
- The Gallium rate [35], $R_{\rm Ga} = (68.0 \pm 3.8)$ SNU, obtained averaging the most recent SAGE, Gallex and GNO data.

- The Chlorine rate [36], $R_{\rm Cl} = (2.56 \pm 0.23)\,{\rm SNU}$.
- The KamLAND reactor anti-neutrino data, divided in 13 energy bins with prompt energy higher than 2.6 MeV [37].

We revised solar model predictions and uncertainties [38] including the recent measurement of the $^{14}{\rm N}(p,\gamma)^{15}{\rm O}$ nuclear cross section [39], which reduces the predicted CNO fluxes by roughly 50%.

Data are compared with predictions forming a $\chi^2$ that takes into account statistical, systematic and theoretical uncertainties (on the total solar neutrino fluxes and on the $^8$B spectrum) and their correlations [38]. We plot the $\chi^2$ as function of the 2 parameters that describe sterile oscillations, marginalizing the full $\chi^2$ with respect to all other sources of uncertainty *including the LMA parameters* $\Delta m^2_{\rm sun}$ and $\theta_{\rm sun}$. This step is of course not performed in usual analyses. Proceeding in a fully numerical way, it would be too demanding for present computers. We can however approximate all observables with a first order Taylor expansion around the best-fit LMA point, since experiments allow only relatively minor shifts from it. In this way marginalization over $\Delta m^2_{12}$ and $\theta_{\rm sun}$ can be performed analytically, using the same Gaussian techniques commonly employed for other 'systematic' parameters. Fig.a 4 shows that performing this linearization (dashed lines) we obtain a satisfactory approximation to the usual active-only global fit of solar neutrinos (continuous lines). With more data this approximation will become more and more accurate.

Solar $\nu$ and reactor $\bar\nu$ data cannot be fit independently, since both sets of data depend on solar oscillation parameters. Inclusion of KamLAND data presents a slight complication: due to poor statistics, the Poissonian distribution must be used. Nevertheless small deviations from the LMA best fit (due to sterile effects and to systematic uncertainties) can be taken into account in Gaussian approximation, obtaining

$$\chi^2 = 2(t - r\ln t) \simeq 2(t_0 - r\ln t_0) + 2\epsilon(t_0 - r) + r\epsilon^2$$

where $r$ are the observed rates and $t = t_0(1+\epsilon)$ the predicted rates. In our analysis $\epsilon$ is the correction due to sterile neutrinos. Fig. 4b shows that we can accurately analytically approximate the usual active-only global fit of solar plus KamLAND data.

## 4.3 Results

We start recalling how LMA oscillations behave in absence of sterile neutrinos [23]. Fig. 5a shows the composition of the two neutrino mass eigenstates. For sake of illustration we assumed normal hierarchy, $m^2_1 \ll m^2_2 \simeq \Delta m^2_{\rm sun} \ll m^2_3 \simeq \Delta m^2_{\rm atm}$. At higher neutrino energies,

$$E_\nu \gg E_* \approx \Delta m^2_{\rm sun}/G_{\rm F}N_e^{\rm sun} \sim \text{few MeV},$$

matter effects dominate around the center of the sun, $r \lesssim 0.2R_{\rm sun}$ where neutrinos are produced as $\nu_e \approx \nu_{2m}$. The LMA level crossing at $r \approx 0.2R_{\rm sun}$ is adiabatic (in fact the solar mixing angle $\theta_{\rm sun}$ is so large that fig. 5 does not look like a level crossing) so that neutrinos produced as $\nu_{2m}$ exit from the sun as $\nu_2 = \sin\theta_{\rm sun}\,\nu_e + \cos\theta_{\rm sun}\,\nu_{\mu,\tau}$ i.e. $P_{ee} = \sin^2\theta_{\rm sun}$. This limit roughly holds at energies probed by SNO and SK: e.g. their total rate is $P_{ee} \approx 1.15\sin^2\theta_{\rm sun}$. At $E_\nu \lesssim E_*$ $P_{ee}$ increases and $\nu_{1m}$ contains some $\nu_e$ because matter effects are no longer dominant. At $E_\nu \ll E_*$

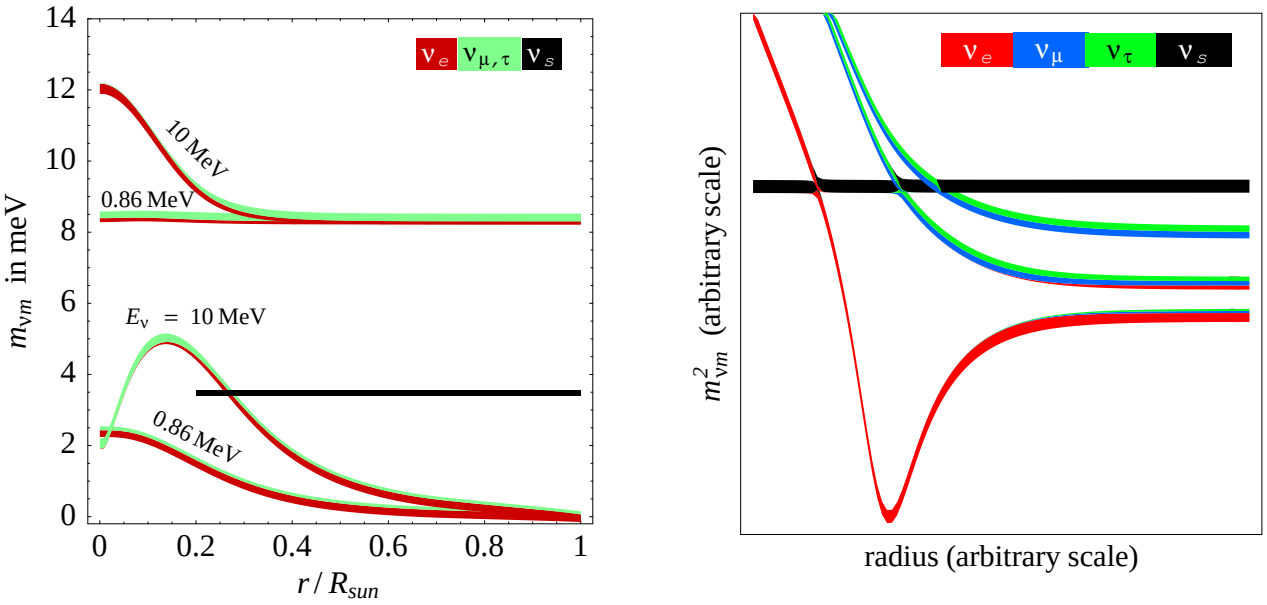


Figure 5: **Level crossing schemes**. *The right plot shows qualitatively the effective anti-neutrino masses in a supernova. The left plot shows the effective neutrino masses in the sun. We assumed hierarchical active neutrinos (i.e. $m_1 = 0$ and $m_2 = (\Delta m^2_{\rm sun})^{1/2}$) and plotted the two matter eigenstates that give rise to LMA oscillations for two different values of $E_\nu$: 10 MeV and 0.86 MeV, the energy of the main Beryllium line. Colors indicate the flavour composition. An extra sterile neutrino with small mixing is represented by an horizontal line with height equal to its mass.*

matter effects are negligible and one gets averaged vacuum oscillations, $P_{ee} = 1 - \frac{1}{2}\sin^2 2\theta_{\rm sun}$. This energy range has been explored by Gallium experiments.

We now discuss how to understand qualitatively the sterile/active mixing effects [23]. If sterile/active mixing is small, the mostly $\nu_{\rm s}$ state is represented by adding one quasi-horizontal line to fig. 5a. Depending on its height (determined by the mass of the sterile neutrino) the mostly sterile level crosses one or none of the two mostly active neutrinos (for all relevant neutrino energies the sterile state does not cross both active neutrinos) after or before the LMA resonance (or after and before). In each case one can understand the behavior of the survival probabilities from the level-crossing scheme: in the example plotted in fig. 5a a neutrino produced at $r_0 \approx 0.2$ experiences a single level crossing at $r_1 \approx 0.3$. This example corresponds to the case considered in [40]: a sterile neutrino weakly mixed with $\nu_1$, with mass splitting $\Delta m^2_{14}$ somewhat smaller than $\Delta m^2_{12}$. A solar $\nu_e$ produced at $r \sim 0.2 R_{\rm sun}$ contains a $\nu_{1m}$ component that crosses the $\nu_{\rm s}$ state once, getting partially converted into $\nu_{\rm s}$. This gives a dip in the survival probability at intermediate energies: at low energies one has averaged vacuum oscillations (negligibly affected by the small sterile mixing angle), at high energies matter effects dominate so that $\nu_e \simeq \nu_{2m}$ that does not cross the sterile level. Fig. 7A,B show examples of this behavior. Even sticking to the case of $\nu_{\rm s}/\nu_1$ mixing, qualitatively different effects are present for other values of the oscillation parameters, studied in fig. 6a. E.g. the example in fig. 7D illustrates the case discussed in [41, 7]:

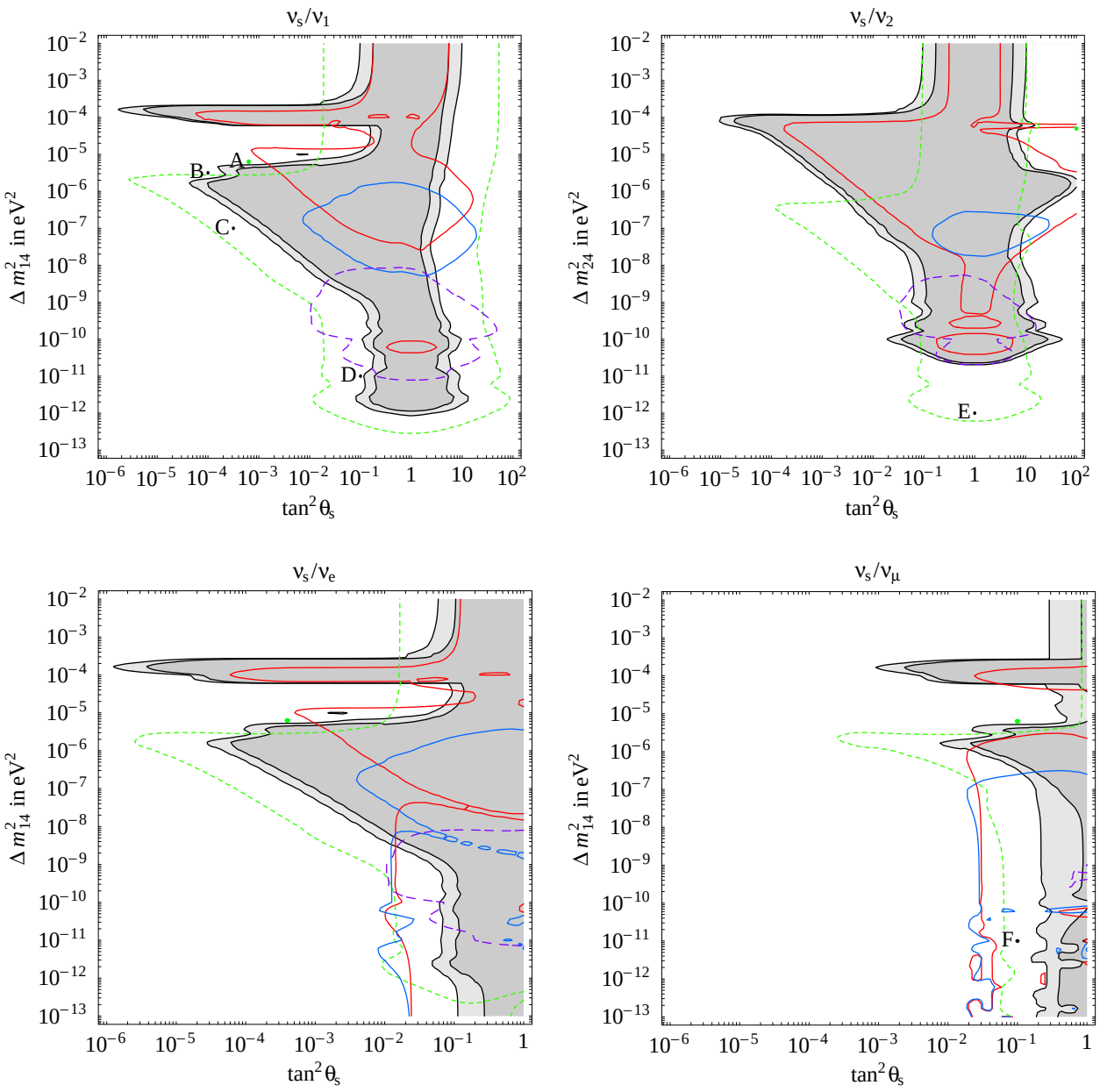


Figure 6: **Sterile mixing: effects in solar neutrinos.** *No statistically significant evidence is found. Shaded regions: excluded at* 90, 99% *C.L. Coloured lines are iso-curves of a few promising signals. Continuous red line:* $A^{\rm ES}_{\rm d/n}$ *differs from LMA by 0.005. Continuous blue line: 0.02 day/night asymmetry at Borexino. Dashed violet line: seasonal variation at Borexino with 0.02 amplitude. Short-dashed green line:* $P_{ee}$ *at sub-MeV energies differs from LMA by 0.02. Other signals are discussed in the text. The letters* A,. . . ,F *indicate sample points, studied in detail in fig. 7.*

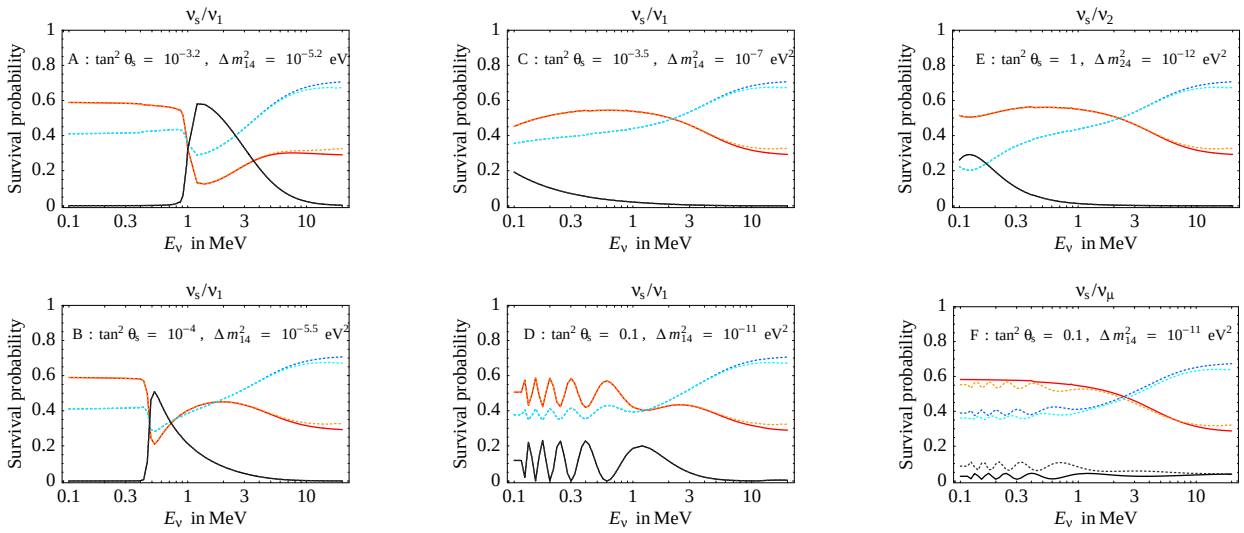


Figure 7: *A few samples of still allowed sterile effects in solar neutrinos. We plot, as function of the neutrino energy, $P(\nu_e \to \nu_e)$ (decreasing red curve), $P(\nu_e \to \nu_{\mu,\tau})$ (increasing blue curve) and $P(\nu_e \to \nu_s)$ (lower black curve). The continuous (dotted) curve are the values during day (night). The sample points* A,. . . , F *are drawn in fig. 6 as dots.*

large $\theta_s$ and small $\Delta m^2_{14} \sim 10^{-12}\,\mathrm{eV}^2$. In all these examples *sterile neutrinos manifest at low energy*, $E_\nu \lesssim E_*$. There is a general reason for this behavior: in absence of sterile effects, only at such energies LMA oscillations allow a $\nu_1$ component in the solar neutrino flux.

We also consider a sterile neutrino mixed with $\nu_2$ or $\nu_3$. $\nu_s/\nu_1$ mixing and $\nu_s/\nu_2$ mixing affect solar neutrinos in similar ways. In fact the $\nu_1^m$ and $\nu_2^m$ neutrino eigenstates in matter both typically contain significant $\nu_1$ and $\nu_2$ components. There are some differences in $\mathcal{O}(1)$ factors, which produce the difference between fig. 6a ($\nu_s/\nu_1$) and b ($\nu_s/\nu_2$). The most evident difference in the shape of the excluded region is due to our choice of the parameterization: when studying $\nu_s/\nu_2$ mixing we produce plots with $\Delta m^2_{24}$ on the vertical axis, so that small values of $\Delta m^2_{24}$ correspond to $\nu_s$ quasi-degenerate with $\nu_2$ (rather than with $\nu_1$).

A sterile neutrino mixed with $\nu_3$ gives much smaller effects in solar neutrinos, so that we do not show the corresponding plot. This happens because matter effects negligibly mix $\nu_3$ with $\nu_{1m}$ or $\nu_{2m}$, so that MSW resonances are highly non adiabatic i.e. ineffective.[11]

As discussed in section 2, sterile mixing with one active mass eigenstate is a special configuration. Therefore we also consider a sterile neutrino mixed with a flavour eigenstate: $\nu_e$, $\nu_\mu$ or $\nu_\tau$. In such a case there are active/sterile oscillations at multiple $\Delta m^2$ values, which (in view of the observed mass differences among active neutrinos) cannot be all small. This is the main difference with respect to the previous case, and implies that sterile oscillation effects are present even for $\Delta m^2_{i4} = 0$. To understand better this point let us consider the case $\Delta m^2_{14} \to 0$. In this

[11]Narrow dips in $P_{ee}(E_\nu)$ are possible close to specific energies such that the mostly sterile state crosses active neutrinos when their position-dependent eigenvalues are maximal. A look at fig. 5a might help to understand this issue.

limit neutrinos exit from the sun as an incoherent mixture of $\nu_2$ and $\nu_1$, which both contain some sterile component. At $E_\nu \gg E_*$ LMA is fully effective and neutrinos exit as pure $\nu_2$, so that vacuum oscillations related to the small $\Delta m^2_{14}$ have no effect. On the contrary, at $E_\nu \lesssim E_*$ there is a $\nu_1$ component which experiences vacuum oscillations with the mostly sterile state. These vacuum oscillations affect the $\nu_e$ flux (if $\nu_{\rm s}$ is mixed with $\nu_e$ as in fig. 6c), or the $\nu_{\mu,\tau}$ flux (if $\nu_{\rm s}$ is mixed with $\nu_{\mu,\tau}$ as in fig. 6d). In general, a mostly sterile state significantly mixed with $\nu_1$ and almost degenerate to it, $\Delta m^2_{14} \sim 10^{-10}\,{\rm eV}^2$, gives significant spectral distortions, *but only below the energy threshold of SK and SNO*. This is illustrated in fig. 7 by the sample points D, E and F.

Fig. 6c studies $\nu_{\rm s}/\nu_e$ oscillations for generic values of $\Delta m^2_{14}$, and is similar to fig. 6a,b apart from the difference discussed above. $\nu_{\rm s}/\nu_\mu$ mixing affects solar neutrinos in the same way as $\nu_{\rm s}/\nu_\tau$ mixing, and both cases give relatively mild effects, as shown in fig. 6d.

It is interesting to notice that there are sizable and specific earth matter effects if the sterile neutrino has a large mixing e.g. with $\nu_e$, and is quasi-degenerate e.g. to $\nu_1$. In fact, the two quasi-degenerate neutrinos have different amounts of active and sterile components; due to matter effects, in the earth the two states are no longer quasi-degenerate, giving oscillations with wave-length $\sqrt{2}\pi/G_{\rm F}N_e^\oplus \sim 6000\,{\rm km}$, comparable to the size of the earth

In all cases fig.s 6 show the regions already excluded at 90 and 99% C.L. (2 dof) by present data (these regions are precisely defined by $\chi^2 > \chi^2_{\rm min} + 4.6$ and 9.2).[12] We emphasize that most of the excluded regions are disfavoured only by combining high-energy (SNO, SK) with low-energy (Gallium) solar data: each kind of data-sets alone tests only a minor region. This means that present data are already able of fixing oscillation parameters with some redundancy, partially testing the LMA hypothesis. Only little regions are excluded if we fit only high-energy data, or only low-energy data. In fact, sterile oscillations that crucially involve $\nu_1$ affect solar neutrinos only at $E_\nu \lesssim E_*$ because only in this energy range the sun emits $\nu_1$.

The other contours in fig.s 6 show which regions can be explored by some future experiments.

- In view of the previous comment it should be not surprising that the relatively more powerful future measurement (dotted green line) is an improved measurement of $P_{ee}$ at sub-MeV energies. Taking into account solar model uncertainties and plans of future experiments, we assumed — maybe optimistically — that it will be possible to see 0.02 shifts from the LMA value of $P_{ee}$.[13]

- The red continuous line shows what can be achieved by measuring the day/night asymmetry (normalized as $2(R_{\rm day} - R_{\rm night})/(R_{\rm day} + R_{\rm night})$) at Boron energies with 0.01 precision in a future Mton water Čerenkov experiment. We have considered this test because the needed experiment seems highly motivated by various other considerations.

[12] Using instead $\chi^2 > \chi^2_{\rm LMA} + 4.6$ and 9.2 would give slightly weaker constraints. One might think that this latter procedure should be preferred because gives more 'robust' bounds. It gives instead under-constraining bounds. More robust bounds should be obtained demanding a higher C.L. to the correct statistical test, rather than inventing 'more robust' tests. A correct 90% C.L. bound does not hold with more than 90% probability.

[13] As in [42] we averaged $P_{ee}$ assuming that *pp* neutrinos will be detected by elastic scattering on electrons; similar results hold for other possible techniques. Assuming that LMA is the end of the story, ref. [42] found that feasible sub-MeV measurements would not have a significant impact on the determination of the oscillation parameters. We here find that sub-MeV measurements are instead crucially important for probing sterile oscillations.

| | $\theta_{\rm ad} \ll \theta_{\rm s} \ll 1$ | $\theta_{\rm s} \sim 1$ |
|---|---|---|
| $m_{\rm s} \gg m_2$ | no effect | $P_{es} \sim 1$ |
| $m_{\rm s} \gtrsim m_2$ | $P_{es} = 1$ at large $E_\nu$, 0 below | $P_{es} \sim 1$ increases at $E_\nu > E_*$ |
| $m_{\rm s} \lesssim m_2$ | no effect | $P_{es} \sim 1$ decreases at $E_\nu > E_*$ |
| $m_{\rm s} \gg m_1$ | peak $P_{es} \sim 1$ at $E \sim E_*$ | $P_{es} \sim 1$ decreases at $E_\nu > E_*$ |
| $m_{\rm s} \gtrsim m_1$ | $P_{es} \sim 1$ decreases at $E_\nu > E_*$ | $P_{es} \sim 1$ decreases at $E_\nu > E_*$ |

Table 1: *Rough classification of possible sterile MSW resonances in the sun. $m_{\rm s}$, $m_1$ and $m_2$ are respectively the masses of the mostly $\nu_{\rm s}$, $\nu_1^{\rm a}$ and $\nu_2^{\rm a}$ states; $E_* \sim$ few MeV is the LMA critical energy and $\theta_{\rm ad} \sim (\Delta m^2/10^{-9}\,{\rm eV}^2)^{1/2}$. No effect is present if $\theta_{\rm s} \ll \theta_{\rm ad}$.*

- Coming to near-future experiments, the other lines show what Borexino (and/or possibly KamLAND) can do by studying (mainly) Beryllium neutrinos. We do not show the impact of a measurement of the total rate, which has a relatively large theoretical error [38][14] and instead focus on signals that LMA predicts to be unobservable. The region inside the continuous blue line has a day/night asymmetry in the Beryllium rate larger than 0.02. In the region inside the dot-dashed blue line the Beryllium rate shows anomalous seasonal variations with amplitude larger than 0.02. The physics behind these effects is similar to the one well known from discussions of LOW and (Q)VO $\nu_e \to \nu_{\mu,\tau}$ oscillations (now excluded).

- We do not show results for a few other signals, that seem less promising than the ones discussed above. One can measure better the energy spectrum of Boron neutrinos, measure Beryllium neutrinos both in NC and CC scatterings, and look for day/night or seasonal variations in *pp* neutrino rates. Active/sterile oscillations with $\Delta m^2 \sim 10^{-5}$ and $\tan^2\theta_{\rm s} \sim 0.1$ can distort the $\bar\nu_e$ energy spectrum in KamLAND or in future reactor experiments.

In table 1 we qualitatively classify how MSW resonances with a sterile neutrino affect solar neutrinos. The main variables are: which state is crossed, how large is the mixing. Fig. 7 shows a few examples of specific oscillation patterns compatible with present data.

## 4.4 Hints and anomalies: solar data

Finally, we have studied if present solar data contain hints of sterile neutrino effects. There are two ways of searching for new effects: data-driven or theory-driven.

In the data-driven approach one performs a goodness-of-fit test, that should reveal if data contain some generic indication for new physics beyond LMA oscillations. In practice, this means carefully looking if data contain hints of anomalous results.[15] Present neutrino data contain the following non-statistically-significant hints:

[14] For values of the oscillation parameters around the 'vertex' of the MSW 'triangle' (at $\Delta m^2_{14} \approx 10^{-5.5}\,{\rm eV}^2$ and $\theta_{\rm s} \approx 10^{-2}$) sterile neutrinos can give a deep dip in $P_{ee}$ at $E_{\rm Be} = 0.863\,{\rm MeV}$. Such effects can significantly reduce the total rate at Borexino compatibly with present data and without giving different kind of signals, such as day/night or seasonal variations.

[15] In the past, global analyses of solar data reported the result of a Person $\chi^2$ test. Today it would tell that even the LOW solution (which has been excluded) is perfectly acceptable. Therefore the fact that, according to the $\chi^2$ test, LMA gives a good fit is not a useful information. In fact, as discussed in [41], the $\chi^2$ test is only sensitive to variations in the $\chi^2$ larger than $\sqrt{N}$, where $N \sim 100$ is the number of data points. In the present

- The rate measured by the Chlorine experiment is 1.4 experimental standard deviations lower than the best-fit value predicted by active-only oscillations.[16]

- The lack of an up-turn in present $\nu_e$ energy spectra does not give a statistically significative hint for new effects additional to LMA oscillations. To get a feeling of how accurately SNO and (mainly) SK data test the energy spectrum around $E_\nu \sim 10\,\mathrm{MeV}$ we fit these data assuming
$$P(\nu_e \to \nu_e) = \sin^2\theta_{\rm sun} + \alpha(\mathrm{MeV}/E_\nu)^2 = 1 - P(\nu_e \to \nu_{\mu,\tau}).$$
At energies probed by SK and SNO LMA oscillations have this form with $\alpha \approx 2$. Data give $\alpha = 1 \pm 2.5$.

- A $2 \div 3\sigma$ indication for sterile neutrinos might appear if analyses that suggest higher values of the nuclear factors $S_{17}(0)$ and $S_{34}(0)$ (and therefore a Boron flux higher than what measured by SNO) were confirmed [43].

- According to some reanalyses, solar neutrino rates of various experiments show some time modulation at specific frequencies. However subsequent analyses performed by some experimental collaborations do not corroborate these claims [44].

The data-driven approach cannot see new physics that manifests giving small corrections to many observables. These diffuse minor effects can be seen if one knows what one is looking for. More precisely, one performs a fit assuming a theory with $n$ extra parameters and looks if the best-fit improves by more than $n$. Our plots in fig.s 6 explore a few $n = 2$ representative slices of the full 4-dimensional parameter space of relevant active/sterile oscillation parameters: various regions (not shown) are favoured in a non statistically significant way. The best fit values, indicated by the green dots in fig.s 6, have a $\chi^2$ lower than best-fit LMA oscillations at most by 3 units. In order to study the general $4\nu$ case we also computed local minima of the $\chi^2$ using numerical minimization techniques. We have not found statistically significant indications for an extra sterile neutrino.

## 4.5 What is the bound on the sterile fraction in solar oscillations?

Assuming that solar neutrinos oscillate into $\nu_e \to \sin\alpha\,\nu_{\rm s} + \cos\alpha\,\nu_{\mu,\tau}$ the question is: what is the bound on the 'sterile fraction' $\eta_{\rm s} \equiv \sin^2\alpha$? We here compare with previous results. Oscillation effects at Boron energies can be parameterized as
$$\Phi_{\nu_e} = \Phi_{\rm B} P_{ee}, \qquad \Phi_{\nu_{\mu,\tau}} = \Phi_{\rm B}(1-P_{ee})(1-\eta_{\rm s}), \qquad \Phi_{\nu_{\rm s}} = \Phi_{\rm B}(1-P_{ee})\eta_{\rm s}. \tag{12}$$
SK and SNO have measured $\Phi_{\nu_e}$ and the total flux of active neutrinos $\Phi_{\nu_{e,\mu,\tau}}$: these two measurements alone cannot determine the three unknown quantities $P_{ee}$, $\eta_{\rm s}$ and $\Phi_{\rm B}$ (unoscillated total Boron flux). Adding the solar model prediction for $\Phi_{\rm B}$ gives
$$\eta_{\rm s} \approx \frac{\Phi_{\rm B} - \Phi_{\nu_{e,\mu,\tau}}}{\Phi_{\rm B} - \Phi_{\nu_e}} \approx 0 \pm 0.2 \tag{13}$$

case $N \gg 1$: this explains why the $\chi^2$ test is so inefficient and one has to perform less standard more efficient tests.

[16] Before revising solar model predictions including the recent LUNA data [39], the Chlorine rate was lower by $1.7\sigma$ (according to our results, in agreement with other similar analyses, see e.g. [40]). The inclusion of LUNA results negligibly affects the global fit of solar and KamLAND data in terms of active/active oscillations.

where $\eta_s$ is small because $\Phi_B$ agrees with the measured total $\nu_{e,\mu,\tau}$ flux. In line of principle this agreement might be accidental: $\Phi_B$ could be larger than what predicted by solar models, and a fraction of it could oscillate into sterile neutrinos leaving a reduced $\Phi_{\nu_{e,\mu,\tau}}$. In view of all other constraints (on spectral distortions, Gallium rates,...) it seems difficult to realize this scenario with oscillations.

Most previous analyses prefer to obtain constraints on $\eta_s$ only from this second argument. They add one sterile neutrino mixed only with $\nu_{\mu,\tau}$ and separated by a large mass splitting: $\Delta m^2_{14} \gg \Delta m^2_{\rm sun}$. This special configuration gives an energy-independent $\eta_s$ and an energy dependence of $P_{ee}$ similar to what obtained for $\eta_s = 0$. This choice does not allow to fit low energy Gallium data together with high energy SNO and SK data: the resulting bound on $\eta_s$ is [2]

$$\eta_s \approx 0 \pm 0.1, \tag{14}$$

somewhat stronger than the bound in eq. (13) obtained using only the solar model prediction for the Boron flux. We stress that this constraint on $\eta_s$ can be relaxed by making milder assumptions on the active/sterile oscillation parameters. For example, even still maintaining $\Delta m^2 \gg \Delta m^2_{\rm sun}$ $\eta_s$ is energy-dependent if the heavy $\nu_s$ mixes with $\nu_e$, or with the mass eigenstate $\nu_1$ ($\eta_s$ is about 2 times larger at lower energy, see fig. 7) or with $\nu_2$ ($\eta_s$ is about 2 times larger at higher energy).

When we focus on the special configuration considered by previous analyses we get $\chi^2(\eta_s = 1/4) - \chi^2(\eta_s = 0) = 8.3$ (including in the fit the BP00 prediction for the total Boron flux) and 6.9 (not including the prediction for the Boron flux: this value of the $\Delta\chi^2$ agrees with other analyses [2]). In fact, in the special configuration our parameter $\theta_s$ is related to the sterile fraction as $\sin^2\theta_s = 2\eta_s$ (for maximal atmospheric mixing). We produced fig. 6 including in our data-set the solar model prediction for the total Boron flux. Dropping it would give only minor modifications, as a comparison of eq. (13) with eq. (14) indicates.

# 5 Sterile effects in supernovæ and other astrophysical sources of neutrinos

Having discussed sterile effects in the sun, it is useful to discuss the analogous effects in core-collapse supernovæ (SN) focussing on the differences between the two cases and emphasizing what one loses and what one gains studying SN neutrinos.

- Present detectors can only study SN neutrinos from our galaxy, and possibly from nearby galaxies: such SN neutrinos have a duty time of $\mathcal{O}(10)$ seconds every $\mathcal{O}(10^9)$ seconds [45, 46]. This makes backgrounds less problematic, but allowed to detect so far only $\mathcal{O}(10)$ SN1987A events [56]. Running solar neutrino experiments could detect thousands of events from a future SN exploding at distance $D \sim 10$ kpc. An even more impressive harvest of data could come from a future Mton water-Čerenkov detector or from other more SN-oriented future projects [47].

- In a SN the matter density grows from zero up to nuclear density ($\rho \simeq 10^{14}\,{\rm g\,cm^{-3}}$) in the stiff inner core: matter effects are important for all the mass range that we consider (up to about $10^2\,{\rm eV}$). In this mass range, and given the typical SN neutrino energy of $\sim 10\,{\rm MeV}$, active/sterile MSW resonances occur outside the neutrino-sphere (roughly

defined as the regions after which neutrinos freely stream, $\rho \ll 10^{12}\,\mathrm{g\,cm^{-3}}$). In particular, conversions inside the neutrino-spheres (which could drain almost all the SN energy) do not take place.[17] We only receive neutrinos that come out of the neutrino-spheres on the side of the SN closer to us. Unlike the case of the sun, it is not necessary to average over the production point, because the production and the oscillation regions are spatially separated.

- While only $\nu_e$ are produced in the sun, SN produce all active $\nu$ and $\bar{\nu}$, roughly in similar amounts [46]. They mix and convert among themselves, and possibly with sterile neutrinos [53, 51, 54, 52]. Present experiments can accurately study $\bar{\nu}_e$. In fact in the energy range $m_e \ll E_\nu \ll m_p$ relevant for SN neutrinos, $\bar{\nu}_e p \to \bar{e} n$ scatterings allows to detect $\bar{\nu}_e$ and to measure their energy. Detecting other neutrinos (e.g. via $\nu e$ scattering, deuterium dissociation, $\nu_e$ absorption on carbon) is possible and future projects could give significant information. In the following, we focus on the $\bar{\nu}_e$ flux.

- $\bar{\nu}_{e,\mu,\tau}$ experience no active/active matter resonance (unlike $\nu_{e,\mu,\tau}$; we are assuming normal hierarchy, and equal initial fluxes of muon and tau-neutrinos): their effective $\Delta m^2$ in matter increases in a monotonous way when the matter density grows. The sterile effect that can more strongly affect the $\bar{\nu}_e$ rate is a low-density $\nu_\mathrm{s}/\nu_1$ MSW resonance, possible when the mostly sterile neutrino is lighter than $\nu_1$ (i.e. $\theta_\mathrm{s} > \pi/4$ in our parameterization).

  Furthermore, due to the peculiar composition of the inner part of the mantle (deleptonized matter) the $\nu_e$ potential changes its sign in the deep region of the mantle, and it does so in a very steep manner [46, 48, 49, 50] (see fig. 5b), adding a MSW resonance also for $\theta_\mathrm{s} < \pi/4$. Although details are uncertain, this is a robust prediction. It implies that $\nu_\mathrm{s}$ always meets a "sharp" resonance with $\bar{\nu}_e$ in the deep region of the mantle [51, 52].

- SN neutrinos are emitted from galactic distances, allowing to probe vacuum oscillations with $\Delta m^2$ as low as $10^{-18}\,\mathrm{eV}^2$ (the precise value depend on the SN and on its distance from the earth: different SN probe different ranges).

  SN neutrino reach energies higher than solar $\nu$, perhaps up to 100 MeV, and could therefore probe earth matter effects and spectral distortions.

- While the sun is essentially static, an exploding SN is a dynamical environment (neutrino light-curve evolution, passage of the shock wave...); including the time dependence in the neutrino fluxes and in the matter density profile is too much demanding and probably useless for our purposes, given the poor knowledge of the details. We focus on a typical SN configuration, which includes all the characteristic features of the SN cooling phase.

  A reliable prediction of the emitted fluxes is still lacking and the explosion mechanism is not yet under control. However, it is relatively easier to predict the $\nu_{e,\mu,\tau}, \bar{\nu}_{e,\mu,\tau}$ energy spectra, which in thermal approximation only depend on their cross sections. On the contrary their total fluxes also depend on the SN density profile; in particular the thermal approximation does not imply equipartition among different flavours. The underlying complexity of SN

[17] The resonances with the sterile state would enter in the neutrino-spheres (in the inner core) for $\Delta m^2 \gtrsim 10^5\,\mathrm{eV}^2$ ($\gtrsim 10^7\,\mathrm{eV}^2$ respectively).

explosions makes hard to reduce theoretical uncertainties, posing a threat on the usefulness of precise SN $\nu$ experiments as tools for studying oscillations.

As a last warning, we have to recall the reluctance of the neutrino data from the only SN we know to fit into a simple and straightforward interpretation. The main reasons are: the energy distribution of Kamiokande and IMB look different; both experiments have an excess of forward events; the 5 LSD events cannot be accounted for.

As for the future, there are various interesting observables, and it is difficult to guess on which signals we should focus. This will probably depend on compromises among future experimental and theoretical capabilities.

Several SN-related bounds on the active/sterile neutrino mixing have been considered in the literature [51, 53, 54, 55]. Focussing on the cooling phase neutrinos, they include (**i**) the detection of $\bar{\nu}_e$ from SN1987a in the Kamiokande and IMB experiments [56], which sets a constraint on the portion of neutrinos that oscillate into $\nu_{\rm s}$; (**ii**) r-process nucleosynthesis: a fraction of the heavy elements in nature is supposed to be synthesized in the region surrounding the core of the exploding stars, provided that the electron fraction $Y_e < 0.5$; even small modifications of neutrino fluxes affect the process, so that the request of a successful nucleosynthesis has been used to set limits (see e.g. [55, 51]); (**iii**) re-heating of the shock: in the delayed-shock/neutrino-driven picture of SN explosion, the flux of neutrinos and antineutrinos from the early stages of the accretion phase (which should carry $10 \div 20$ % of the total flux) are responsible for the actual explosion of the star, pushing from below the stalling shock wave; since $\nu_e$ and $\bar{\nu}_e$ are the most effective in this (interacting with charged and neutral currents with baryonic matter), a cut of their flux would prevent this mechanism from working [51, 54, 57]; (**iv**)... We will only consider the bound from direct observation, which we consider robust enough.[18]

## 5.1 Technical details

The analysis of SN neutrinos can be carried on in a way similar to that of solar neutrinos, after adapting the computational procedure to SN peculiarities, which introduce some complications and allow some simplifications. We must follow the fate of the neutrinos emitted from neutrinospheres along their travel through the star matter, the vacuum and the earth. The density matrix formalism, already described in the 'solar' section 4.1, automatically handles the complication that the SN initial neutrino flux has a mixed flavour composition. In the SN case one should follow the evolution of two $4 \times 4$ density matrices: $\rho(E_\nu)$ for neutrinos, and $\bar{\rho}(E_\nu)$ for antineutrinos. We focus on the total $\bar{\nu}_e$ rate, as measured by $\bar{\nu}_e p$ scatterings with the cuts and efficiency of the KamiokandeII experiment. The cross section is taken from [58].

MSW resonances affect the neutrino density matrix, possibly introducing off-diagonal elements which are however averaged to zero by large oscillation phases. Therefore we can combine probabilities rather than quantum amplitudes: the $4 \times 4$ density matrix can be replaced by

[18] Indeed, for instance, alternative sites for effective nucleosynthesis have been repeatedly proposed. Moreover, the position of such a bound could depend quite heavily on the complicated details of SN dynamics and, in addition, on the interplay of sterile oscillations with it, see below. On the same footing, since the details and the nature itself of the neutrino-driven explosion mechanism are still to be fully understood, we do not consider it here as a robust constraint, not mentioning that it would require a demanding understanding and simulation of the evolution of the SN mantle.

a 4-vector containing its diagonal elements, $\Phi = (\rho_{11}, \rho_{22}, \rho_{33}, \rho_{44})$ and the evolution equation $\rho = \mathscr{U} \cdot \rho^0 \cdot \mathscr{U}^\dagger$ ($\mathscr{U} = \mathscr{U}_n \cdots \mathscr{U}_1$) by [53]

$$\Phi = \mathscr{P}_n \cdots \mathscr{P}_1 \cdot \Phi^0 \qquad \text{where} \qquad (\mathscr{P}_n)_{ij} = |(\mathscr{U}_n)_{ij}|^2 \tag{15}$$

are $4 \times 4$ matrices of conversion probabilities. At the production region, matter effects are dominant, so that matter eigenstates coincide with flavour eigenstates (up to a trivial permutation): $\Phi^0 = (\Phi^0_{\bar{\nu}_s}, \Phi^0_{\bar{\nu}_e}, \Phi^0_{\bar{\nu}_\tau}, \Phi^0_{\bar{\nu}_\mu})$. $\Phi$ are the fluxes of neutrino vacuum eigenstates reaching the earth surface, related to the fluxes of flavour eigenstates by an incoherent sum weighted by the the neutrino mixing matrix $V$:

$$\left(\Phi_{\bar{\nu}_e}, \Phi_{\bar{\nu}_\mu}, \Phi_{\bar{\nu}_\tau}, \Phi_{\bar{\nu}_s}\right)_\alpha = \sum_i |V_{\alpha i}|^2 \Phi_i \tag{16}$$

If neutrinos cross the earth, earth matter effects [59] may reintroduce coherencies among the various fluxes, and one must return to the general quantum expression. Similarly, if two states have $\Delta m^2 \lesssim 10^{-18}\,\mathrm{eV}^2$ vacuum oscillations do not give large phases: evolution in the outer region of the SN and in vacuum must be described keeping the off-diagonal components of the matrix density. In practice, we found convenient to evolve the density matrix in the instantaneous mass eigenstate basis, setting to zero its off diagonal elements when they accumulate large phases. This procedure is described in greater detail in the 'atmospheric' section 6.1.

The effect of active/active oscillations is well known [59]: the LMA resonance is adiabatic and partially swaps active neutrinos, giving[19]

$$\Phi^{\text{after}}_{\bar{\nu}_e} = \cos^2\theta_{\text{sun}} \Phi^{\text{before}}_{\bar{\nu}_e} + \sin^2\theta_{\text{sun}} \Phi^{\text{before}}_{\bar{\nu}_{\mu,\tau}} \qquad \Phi^{\text{after}}_{\nu_e} = \sin^2\theta_{\text{sun}} \Phi^{\text{before}}_{\nu_e} + \cos^2\theta_{\text{sun}} \Phi^{\text{before}}_{\nu_{\mu,\tau}} \tag{17}$$

Active/sterile MSW resonances can occur after of before the LMA resonance.

Concerning the initial fluxes, the accurate results of simulations are usually empirically approximated by a so called "pinched" Fermi-Dirac spectrum for each flavor $\alpha = \nu_e, \bar{\nu}_e, \nu_x$ ($\nu_x$ collectively denotes $\nu_{\mu,\tau}, \bar{\nu}_{\mu,\tau}$) [60, 46]

$$\frac{d\Phi_{\nu_\alpha}}{dt\, dE_\nu}(E_\nu, t) = N(\eta_\alpha) \frac{120}{7\pi^4} \frac{L_\alpha}{T_\alpha^4} \frac{E_\nu^2}{e^{E_\nu/T - \eta_\alpha} + 1} \tag{18}$$

where the pinching parameter $\eta_\alpha$ takes the typical values $\eta_{\nu_e} \sim 5 - 3$, $\eta_{\bar{\nu}_e} \sim 2.5 - 2$, $\eta_{\nu_x} \sim 0 - 2$. For $\eta_\alpha = 0$ the normalization factor is $N = 1$ and $T = \langle E_\nu \rangle / 3.15$. Based on the recent results of [61], we adopt the following average energies and total luminosities for the various neutrino components at the time of the snapshot of fig. 8 (see below)

$$\begin{array}{lll} \langle E_{\nu_e} \rangle \simeq 12\,\mathrm{MeV}, & \langle E_{\bar{\nu}_e} \rangle \simeq 14\,\mathrm{MeV}, & \langle E_{\nu_x} \rangle \simeq 14\,\mathrm{MeV} \\ L_{\nu_e} \simeq 30 \cdot 10^{51}\,\mathrm{erg\,sec}^{-1}, & L_{\bar{\nu}_e} \simeq 30 \cdot 10^{51}\,\mathrm{erg\,sec}^{-1}, & L_{\nu_x} \simeq 20 \cdot 10^{51}\,\mathrm{erg\,sec}^{-1}. \end{array} \tag{19}$$

In accordance with numerical calculations, we shall assume that the ratios of luminosities do not vary much during the whole emission. The initial flux of sterile neutrinos is assumed to

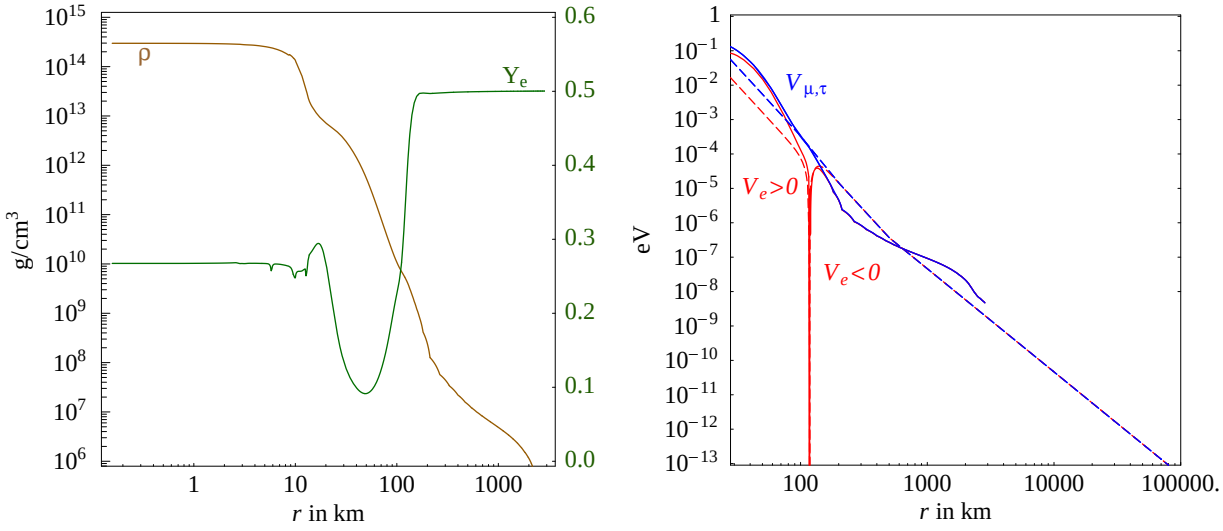


Figure 8: **Supernova profile**. *Fig. 8a: Density $\rho(r)$ and electron fraction $Y_e(r)$ from [50]. Fig. 8b: matter potentials in the SN, for $\bar{\nu}_e$ (red solid line) and for $\bar{\nu}_{\mu,\tau}$ (blue solid line). The dashed lines are the analytic modelization that we adopt.*

be vanishing, as a consequence of the fact that matter oscillations only take place out of the neutrinosphere.[20]

Neutrinos traveling in the SN matter experience the MSW potentials [23, 31]

$$\begin{aligned} V_e &= \sqrt{2} G_{\rm F} n_B \left(3Y_e - 1\right)/2, \qquad & V_\tau &= V_\mu + V_{\mu\tau}, \\ V_\mu &= \sqrt{2} G_{\rm F} n_B \left(Y_e - 1\right)/2, \qquad & V_{\rm s} &= 0, \end{aligned} \tag{20}$$

where $n_B$ is the baryon number density ($n_B = \rho/m_N$ where $m_N \approx 939\,\text{MeV}$ is the nucleon mass[21]) and $Y_e = (N_{e^-} - N_{e^+})/n_B$ is the electron fraction per baryon. Antineutrinos experience the same potentials with opposite sign.

The difference $V_{\mu\tau}$ in the $\nu_\mu$ and $\nu_\tau$ potentials, which appears at one loop level due to the

[19] We are assuming normal hierarchy and $\theta_{13} = 0$. The situation becomes more complicated if instead $\theta_{13} \gtrsim 1^\circ$, because the atmospheric resonance starts changing the result in eq. (17). For $1^\circ \ll \theta_{13} \ll 1$ it is adiabatic. If $\Delta m^2_{23} > 0$ (normal hierarchy) it affects only neutrinos by giving a full conversion, $\Phi^{\rm after}_{\nu_e} = \Phi^{\rm before}_{\nu_{\mu,\tau}}$. If instead $\Delta m^2_{23} > 0$ (inverted hierarchy) it affects only anti-neutrinos, by giving a full conversion, $\Phi^{\rm after}_{\bar{\nu}_e} = \Phi^{\rm before}_{\bar{\nu}_{\mu,\tau}}$.

[20] To be precise, shortly after the collapse the electron neutrino matter potential in the very center of the core is positive, due to the contribution of the trapped neutrinos themselves. This configuration lasts for a short transient period, until the neutrino diffusion depletes their abundance and carries the potential to negative values, where it stays. A small fraction of the electron (anti)neutrinos produced in the deep core could then oscillate into sterile states and constitute a non vanishing flux injected in the mantle.

[21] For the very high densities closer to the core, $m_N$ should be replaced by a (quite different) effective nucleon mass. We can neglect this refinement in the regions of our interest.

different masses of the muon and tau leptons [62], is, according to the SM

$$V_{\mu\tau} = \frac{3G_{\rm F}^2 m_\tau^2}{2\pi^2}\left[2(n_p+n_n)\ln\left(\frac{M_W}{m_\tau}\right) - n_p - \frac{2}{3}n_n\right]. \qquad (21)$$

The effect is not irrelevant in the inner dense regions: for densities above $\rho \sim 10^8\,{\rm g\,cm^{-3}}$, the $\mu\tau$ vacuum mixing is suppressed.

A crucial point concerns the characteristic of the matter density and of the electron fraction in the mantle of the star. We adopt the profiles represented in fig. 8 [50] and we model them with analytic functions that preserve their main features.[22] Namely, the density profile decreases according to a power law $r^{-4}$ out of the $\sim 10\,{\rm km}$ inner core (where instead it has a roughly constant, nuclear density value). At much larger distances the density profile gets modified in a time-dependent way by the passage of the shock wave. Present simulations have difficulties in reproducing this phenomenon and therefore cannot reliably predict the density profile in the outer region. Therefore for $r \gtrsim 500\,{\rm km}$ we assume a power law $\rho = 1.5\ 10^4 (R_\odot/r)^3 {\rm g/cm^3}$, which roughly describes the static progenitor star.

The peculiar $Y_e$ profile in fig. 8 is inevitably dictated by the deleptonization process [49, 48]: behind the shock wave which has passed in the mantle matter, the electron capture on the newly liberated protons is rapid, driving $Y_e$ to low values ($\sim 1/4$). In the outer region, where the density is sensibly lower, the efficiency of the capture is much lower, so that $Y_e$ essentially maintains the value $\sim 1/2$ typical of normal matter. This is important because the matter potential $V_e$ of electron (anti)neutrinos flips sign, see eq. (20), when, in the deep region of the mantle $Y_e$ steeply decreases below 1/3. On the contrary, at this point the matter potentials of muon and tau (anti)neutrinos are marginally affected. Both are plotted in fig. 8.

The data refer to $\sim$0.3 sec after bounce for a typical star of $\sim 11$ solar masses. The subsequent evolution is supposed to move the wave of the $Y_e$ profile slightly outwards, maintaining, however, its characteristic shape. The slight dependence on the progenitor mass, in turn, is not really relevant [63].

This SN density profile has been computed [50] in absence of sterile neutrinos effects. Adding a sterile neutrino, $\nu_e \to \nu_{\rm s}$ conversions can reduce $Y_e$ due to a non-trivial feedback mechanism on the MSW potential experienced by neutrinos [51, 55]. This could even create a new intermediate region with $Y_e < 1/3$, thus introducing two more level-crossing in the $\bar\nu_e$ channel. We neglect these possible extra MSW resonances because they do not affect the $\bar\nu_e$ rate when they are both adiabatic, or both fully non adiabatic.

In summary, although the profiles that we adopt come from a specific computation and refer to a specific instant in time, they incorporate the peculiar features that are important for our purposes. A more refined treatment of this point (later times behavior of the profiles, fine structures connected with the passage of the shock wave...) would of course require to obtain first a complete simulation of the SN evolution, including the explosion. This could be needed to describe the signal from a future supernova, but seems unnecessarily complicated for SN1987A.

## 5.2 Results

Active/sterile mixing significantly affects SN neutrinos for $\theta_{\rm s} \sim 1$. Due to MSW resonances, significant effects can also be present for small mixing, i.e. $\theta_{\rm s} \to 0$ and $\theta_{\rm s} \to \pi/2$. The re-

[22] We thank Adam Burrows for having provided us with the data, and for useful discussions.

cently established active/active mixings are not taken into account in older studies [53, 54] (see however [52]). To understand the main features it is useful to look at the pattern of possible level crossings, qualitatively depicted in fig. 5b at page 18. The three mostly active anti-neutrino eigenstates depend on the radius $r$ as dictated by their measured masses and mixings (we assume $\theta_{13} = 0$ and normal hierarchy) and by the predicted SN density profiles, and are represented in fig. 5b by the three colored curves. The mostly sterile neutrino is generically represented by an almost-horizontal line, which is plotted in fig. 5b in the specific case of small $\bar{\nu}_e/\bar{\nu}_{\rm s}$ mixing and $\Delta m^2_{14} \gg \Delta m^2_{\rm atm}$. There are three possible kinds of active/sterile MSW resonances [51, 52, 53, 54]:

1. The mostly $\bar{\nu}_{\rm s}$ eigenstate crosses the mostly $\bar{\nu}_e$ eigenstate at $r \sim 100\,{\rm km}$, where $V_e$ flips sign. At this point matter effects dominate over active neutrino masses, so that active mass eigenstates coincide with flavour eigenstates. Since $V_e$ flips sign in a steep way this resonance is effective only if $\Delta m^2_{14} \gtrsim 10^{-1\div 0}\,{\rm eV}^2$ (different SN simulations gives values in this range).

2. If the mostly sterile eigenstate is the lightest one (in our parameterization this needs $\theta_{\rm s} \gtrsim \pi/4$) the two eigenstates in 1. cross again at larger $r$. Pictorially, this second resonance is present when the sterile black line is lower than what assumed in fig. 5b. This MSW resonance occurs at large $r$ where $V_e$ is smooth, so that it is effective down to $\Delta m^2_{14} \gtrsim 10^{-6\div 8}\,{\rm eV}^2$. Again, the significant uncertainty is due to uncertainties on the SN density gradient.

3. If instead the mostly sterile eigenstate is the heaviest or the next-to-heaviest state, it crosses one or both of two mostly $\bar{\nu}_{\mu,\tau}$ eigenstates. This is the case illustrated in fig. 5b. The values of $\Delta m^2_{24}$ and $\Delta m^2_{34}$ determine at which $r$ these crossings takes place, and consequently the flavour composition of the mostly active states at the resonance. Entering in the SN, the small $\bar{\nu}_e$ component of $\bar{\nu}^m_{2,3}$ disappears as soon as $V_e - V_\mu$ dominates over $\Delta m^2_{\rm sun}$.[23] The color of mass eigenstates in fig. 5b illustrates these phenomena. In any case, active/sterile MSW resonances with the mostly $\bar{\nu}_{\mu,\tau}$ states do not significantly affect the $\bar{\nu}_e$ rate, see eq. (17).

These considerations allow to understand fig.s 9, where we plot our results for the reduction of the $\bar{\nu}_e$ rate due to sterile mixing.

Let us start from fig. 9a that studies $\nu_1/\nu_{\rm s}$ mixing. Resonance 1 gives a sizable reduction in region 1 of fig. 9a and resonance 2 gives a sizable reduction in region 2. Had we ignored solar mixing the maximal deficit would have been 100%, while in presence of solar oscillations the maximal effect is a $\sim 80\%$ deficit (see also [52]). More precisely, in the interior of region 1 one obtains $\Phi_{\bar{\nu}_e} = \sin^2\theta_{\rm sun}\Phi^0_{\bar{\nu}_e}$ because resonances 1 and 3 are fully adiabatic. In the interior of region 2 one obtains $\Phi_{\bar{\nu}_e} = \sin^2\theta_{\rm sun}\Phi^0_{\bar{\nu}_{\mu,\tau}}$ because resonance 2 is fully adiabatic and resonance 1 irrelevant. Therefore, given the assumed initial fluxes, the $\bar{\nu}_e$ rate gets reduced slightly more strongly in region 2 than in region 1.

In region 12 both resonances 1 and 2 are effective, and tend to compensate among each other: resonance 1 converts $\bar{\nu}_e$ into $\bar{\nu}_{\rm s}$ and resonance 2 reconverts $\bar{\nu}_{\rm s}$ into $\bar{\nu}_e$. In region 3, resonances 3 gives a 20% suppression of the $\bar{\nu}_e$ rate, that sharply terminates when $\Delta m^2_{14} < \Delta m^2_{\rm sun}$. This is

[23] When $V_\mu - V_\tau$ dominates over $\Delta m^2_{\rm atm}$ the flavour composition varies from $\bar{\nu}_\mu \pm \bar{\nu}_\tau$ to $\bar{\nu}_\mu$ and $\bar{\nu}_\tau$. This active/active resonance happens at so high densities that is not relevant for our purposes.

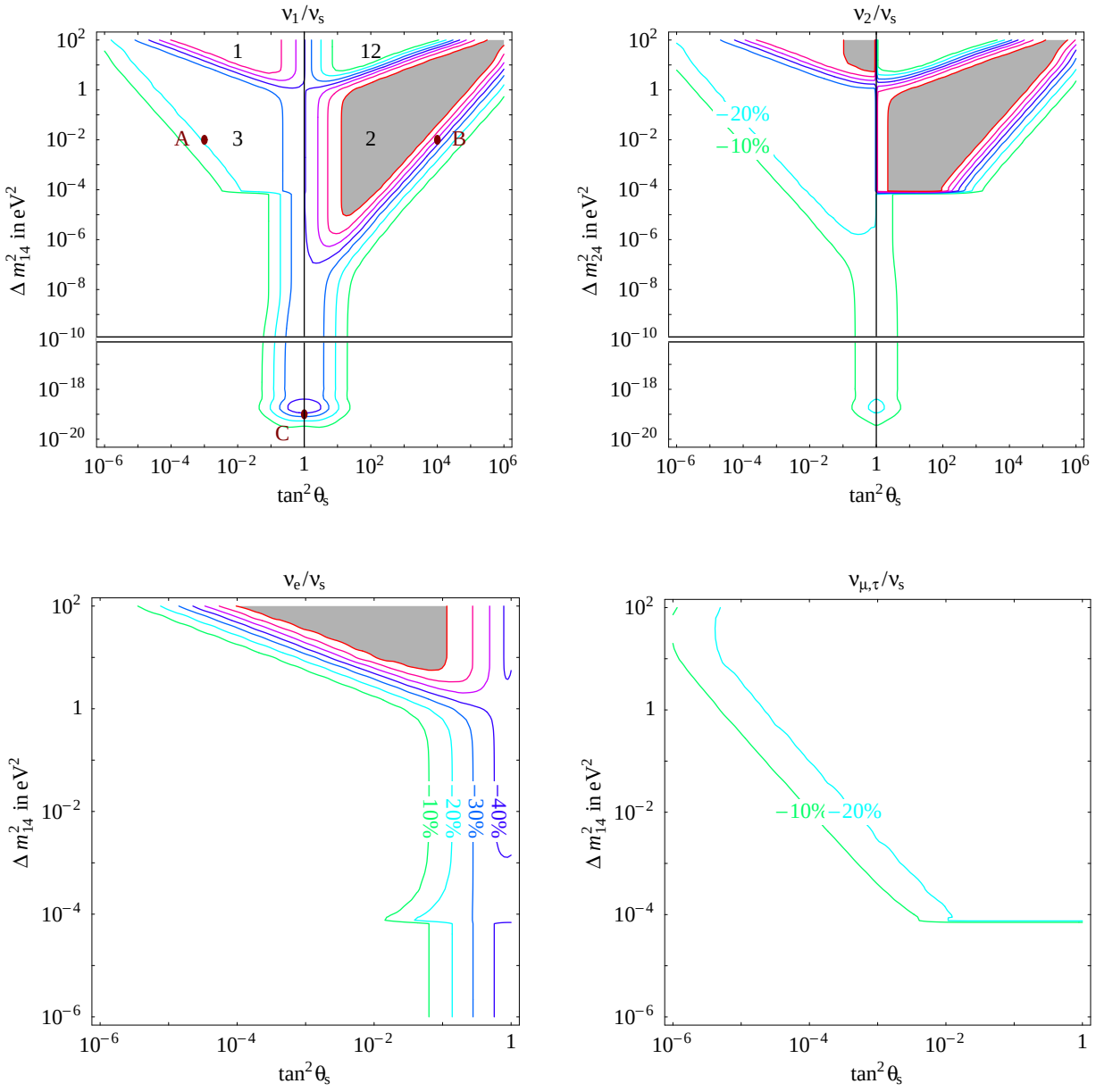


Figure 9: **Sterile effects in supernovæ.** *The iso-contours correspond to a* 10, 20, 30, 40, 50, 60, 70 % *deficit of the SN* $\bar{\nu}_e$ *total rate due to oscillations into sterile neutrinos. The deficit is measured with respect to the rate in absence of active/sterile oscillations and in presence of active/active oscillations (which reduce the no-oscillation rate by* $\sim 10\%$*). We shaded as disfavoured by SN1987A data regions with a deficit larger than* 70%*. While the qualitative pattern is robust, regions with MSW resonances can shift by one order of magnitude in* $\Delta m^2$ *using different SN density profiles.* $\bar{\nu}_3/\bar{\nu}_s$ *mixing (not plotted) does not give significant effects. Fig. 10 studies in detail the sample points here marked as* A, B, C, *and the regions 1, 2, 12, 3 are discussed in the text.*

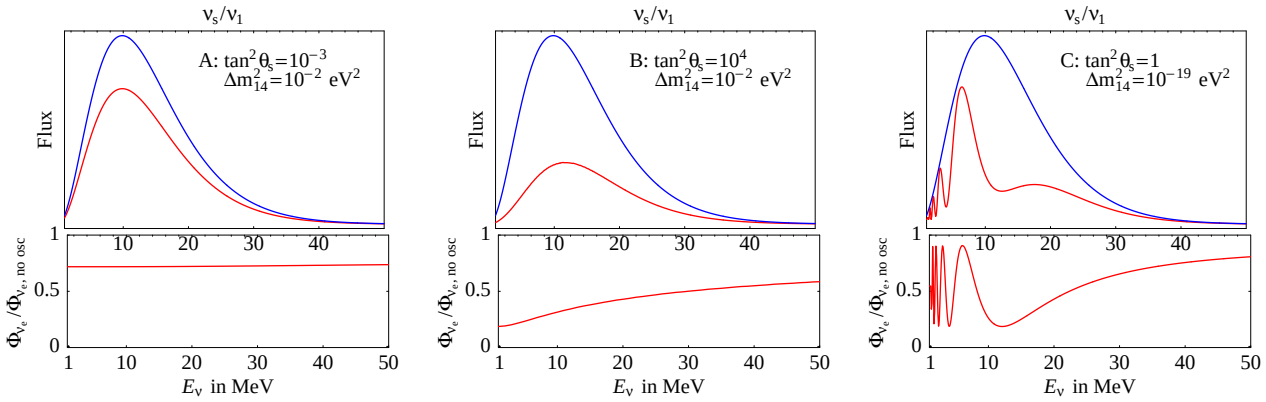


Figure 10: **Sterile effects in supernovæ.** *Distortion of the $\bar{\nu}_e$ flux at sample points* A, B, C.

due to a strong suppression of the mostly $\bar{\nu}_{\mu,\tau}$ eigenstates, which due to solar oscillations would give a 20% contribution to the $\bar{\nu}_e$ rate (ignoring solar mixing, there would be no suppression of the $\bar{\nu}_e$ rate in region 3). This reduction of the $\bar{\nu}_{\mu,\tau}$ fluxes induced by resonances 3 could be better probed by measuring the NC rate (which gets a $\lesssim 40\%$ reduction) and, if neutrinos cross the earth, by distortions of the $\bar{\nu}_e$ energy spectrum. At smaller $\Delta m^2$ and around maximal mixing vacuum oscillations can reduce the $\bar{\nu}_e$ rate by $\lesssim 50\%$: their effect persists down to $\Delta m^2 \sim E_\nu/D \sim 10^{-18}\,\mathrm{eV}^2$. The precise value depends on the distance $D$ (we assumed $D = 10$ kpc).

The other mixing cases are understood in similar ways. We remind that our parametrization is discontinuous at $\theta_\mathrm{s} = \pi/4$: this is reflected in fig. 9b, where we consider $\nu_2/\nu_\mathrm{s}$ mixing. Resonance 2 sharply terminates when $\Delta m^2_{24} < \Delta m^2_{\mathrm{sun}}$. Up to these differences, this case is quite similar to the previous one, because $\bar{\nu}_1$ and $\bar{\nu}_2$ get strongly mixed by matter effects.

On the contrary $\nu_3/\nu_\mathrm{s}$ mixing (not shown) does not give a significant reduction of the $\bar{\nu}_e$ rate. Mixing with the flavour eigenstates behaves in a similar way. Namely, the $\nu_{\mu,\tau}/\nu_\mathrm{s}$ figure shows the reduction in region 3 due to resonances 3, and the $\nu_e/\nu_\mathrm{s}$ figure shows the reduction in region 1 due to resonance 1. The additional feature at $\Delta m^2_{14} \sim \Delta m^2_{\mathrm{sun}}$ is due to adiabatic conversion (for large sterile angles) between the mostly-sterile state and $\nu_2$, that are almost degenerate in this condition. For larger $\Delta m^2_{14}$, there is no $\bar{\nu}_e$ component in $\bar{\nu}_2^m$ so that the crossing is totally non adiabatic, while for smaller $\Delta m^2_{14}$ the two states are separated. As in the solar case, sterile effects persists at all values of $\Delta m^2_{14}$, even if it is small. Unlike in the solar case, such effects are not sensitive to vacuum oscillations (i.e. $\Delta m^2 \sim E_\nu/D \sim 10^{-18}\,\mathrm{eV}^2$) because in a SN neutrinos of all energies experience the adiabatic LMA resonance. Therefore in the lower row of fig.s 9 we only show results at $\Delta m^2_{14} > 10^{-6}\,\mathrm{eV}^2$; nothing changes at smaller values.

SN1987A data can be precisely compared with expectations doing an event by event fit [64]; however the result strongly depends on the assumed average energies and total luminosities of the initial fluxes. The data do not permit detailed studies of the energy distribution. Even more, they cannot discriminate in a significant way between a larger total flux with smaller average energy and a smaller flux with higher average energy. In absence of a quantitative estimation of theoretical uncertainties, and in view of the doubtful aspects of SN1987A data

discussed previously, today we cannot derive precise constraints. Therefore we simply shaded as 'disfavoured' regions where sterile effects reduce the $\bar{\nu}_e$ rate by more than 70%. This is nothing more than a reasonable arbitrary choice.

Future data will permit to know precisely the total rate of $\bar{\nu}_e$ events, and also its distribution in energy and time. The most important single observable could be the average $E_{\bar{\nu}_e}$ energy, or more generically the energy spectrum. Rather than showing iso-contour plots of $\langle E_{\bar{\nu}_e} \rangle$ we describe their main features. In absence of sterile oscillations we expect $\langle E_{\bar{\nu}_e} \rangle \approx 15\,\mathrm{MeV}$. Along the 'diagonal sides of the MSW triangles' 1 and 2 (e.g. around our sample point B) the average energy increases up to $\langle E_{\bar{\nu}_e} \rangle \approx 18\,\mathrm{MeV}$. Along the 'diagonal sides of the MSW triangle' 12 it can decrease down to $\langle E_{\bar{\nu}_e} \rangle \approx 11\,\mathrm{MeV}$. Vacuum oscillations can give the well known distortions of the spectrum, as exemplified in fig. 10C. These effects seem larger than experimental and theoretical uncertainties. In all other cases sterile effects give a quasi-energy-independent suppression of the $\bar{\nu}_e$ rate, and therefore negligibly affect $\langle E_{\bar{\nu}_e} \rangle$. Fig. 10A gives an example. Of course, the average energy of positrons generated by $\bar{\nu}_e p \to n\bar{e}$ scatterings is higher than $\langle E_{\bar{\nu}_e} \rangle$ because the cross section increases with energy.

We focused on supernova antineutrinos. The analogous plots for neutrinos cannot obtained from our $\bar{\nu}$ plots by flipping $\tan\theta_\mathrm{s} \to 1/\tan\theta_\mathrm{s}$, because we are taking into account the effects of active/active oscillations. Effects in neutrinos are more similar to what happens to solar $\nu_e$.

## 5.3 Hints and anomalies: supernovæ

To conclude, we list hints of anomalous effects possibly related to sterile effects in SN neutrinos:

- In the past, the initial SN neutrino fluxes in different flavours were believed to follow an almost exact equipartition of the energy and have gaps in neutrino temperatures larger than in eq. (19) (typical values were $13, 16, 23\,\mathrm{MeV}$ [46]). Under these assumptions SN1987A data, which point to a lower average energy, disfavor solar oscillations with large mixing angle ($\sin^2 2\theta_\mathrm{sun} < 0.9$ at 99% C.L. [65]) while solar data established the relatively large mixing $\sin^2 2\theta_\mathrm{sun} \approx 0.8$. The tension strongly depends on the initial temperatures, and disappears assuming the more recent values in eq. (19) [65].

- Pulsar motion. It has been proposed that the resonant (or non resonant [66]) conversion of sterile neutrinos could explain the observed large proper velocity of newly born neutrons stars [67]. Indeed, in presence of very strong and axially oriented magnetic fields, which could be plausible in the NS environment, the MSW potential includes a contribution (at one loop, from neutrino scattering on the polarized medium) which depends on the relative angle between the neutrino momentum and the magnetic field; this leads to an asymmetric neutrino emission, which could be enough to account for the observed velocities. This mechanism needs sterile neutrinos with keV-scale masses and $\theta_\mathrm{s} \lesssim 10^{-7}$.

- r-process nucleosynthesis [55]: $\nu_e \to \nu_\mathrm{s}$ conversions in the mantle of the star could drive $Y_e$ to low values and have thus been proposed to provide a favorable environment for r-process nucleosynthesis. The relevant range of $\nu_e/\nu_\mathrm{s}$ mixing parameters spans $\Delta m^2 \sim (1 \div 10^2)\,\mathrm{eV}^2$ and $\sin^2 2\theta_\mathrm{s} \sim 10^{-3} \div \mathrm{few}10^{-1}$, which should be checked against the bounds

from cosmological probes that we discussed in the present paper. In the same region, the "conversion plus re-conversion" of antineutrinos instead guarantees that the SN $\bar{\nu}_e$ is not dramatically affected.

## 5.4 Neutrinos from other astrophysical sources

Different kinds of experiments will try to detect neutrinos emitted by extragalactic sources, such as active galactic nuclei. There are no firm expectations. In particular we do not know if the fluxes of these neutrinos will be detectably large, and eventually in which energy range. However, since these neutrinos are presumably mostly generated by $\pi$ decays, like atmospheric neutrinos, one expects similar fluxes of $\nu$ and $\bar{\nu}$ with flavour ratio $e : \mu : \tau \sim 1 : 2 : 0$ (this expectation might be wrong). Atmospheric oscillations then convert the flavour ratio into $1 : 1 : 1$, which is blind to other active/active oscillations.

In presence of an extra sterile neutrino, the $e : \mu : \tau : \mathrm{s} \sim 1 : 1 : 1 : 0$ flavour ratio is not blind to extra active/sterile oscillations. Sterile oscillations can reduce the fluxes of active neutrinos, and vary the relative flavour proportion. Since the total initial fluxes and energy spectra are unknown, and since experiments will probably be able of tagging $\mu$ and maybe $\tau$ neutrinos well [68], we focus only on the observable $\Phi_\mu/\Phi_\tau$.

We assume that the baseline, about 100 Mpc, is much longer than all oscillation lengths. In such a limit the oscillation probability reduces to multiplication of probabilities (rather than of quantum amplitudes):

$$P(\nu_\ell \to \nu_{\ell'}) = P(\bar{\nu}_\ell \to \bar{\nu}_{\ell'}) = \sum_{i=1}^{4} |V_{\ell i}|^2 |V_{\ell' i}|^2 \tag{22}$$

One can verify that sterile mixing with a flavour eigenstate $\nu_\ell$ ($\ell = e$ or $\mu$ or $\tau$) mainly gives a depletion of $\Phi_\ell$. However, as discussed in the rest of this paper, in such a case large active/sterile mixing angles are already disfavoured by other data, so that it is not possible to get a sizable effect.

Present data allow large active/sterile mixing with mass eigenstates $\nu_i$ ($i = 1$ or 2 or 3) if $\nu_\mathrm{s}$ and $\nu_i$ are quasi-degenerate, with $\Delta m^2 \ll 10^{-9}\,\mathrm{eV}^2$. In view of the long base-line, neutrinos from cosmic sources are affected by oscillations with $\Delta m^2 \gtrsim 10^{-17}\,\mathrm{eV}^2$. However each of the mostly active mass eigenstates contains roughly equal component of $\nu_\mu$ and $\nu_\tau$ (unless the atmospheric mixing angle is non-maximal, or unless $\theta_{13}$ and the CP-phase significantly differ from zero): therefore $\nu_\mathrm{s}/\nu_i$ oscillations do not significantly affect $\Phi_\mu/\Phi_\tau$.

In conclusion, near-future experiments that will try to discover neutrinos from cosmic sources do not seem to allow promising searches of sterile neutrino oscillations. See also [69].

Eq. (22) also allows to study vacuum oscillation effects in other kinds of cosmological neutrinos:

- In a near future it seems possible to detect the $\bar{\nu}_e$ emitted by **past core-collapse supernovæ**. At the moment we only have order-of-magnitude predictions, but future SN experiments and studies might allow to better predict their total flux or spectrum. SK almost reached the apparently necessary sensitivity, and it seems possible to improve the

efficiency of tagging neutrons emitted in $\bar{\nu}_e p \to \bar{e} n$ scatterings [70]. Relic SN $\bar{\nu}_e$ are affected by oscillations in the SN (as discussed in the previous section) and by oscillations in vacuum (down to $\Delta m^2 \gtrsim 10^{-25}\,\mathrm{eV}^2$).

- In a far future, it might be possible to directly detect **CMB neutrinos** by coherent scatterings. This would allow to probe oscillations down to $\Delta m^2 \sim 10^{-30}\,\mathrm{eV}^2$.

# 6 Sterile effects in atmospheric, reactor and beam neutrinos

In this section we discuss how SK, K2K, MACRO, CHOOZ, BUGEY, CDHS, CCFR, KARMEN, NOMAD, CHORUS and future experiments of these kinds probe sterile oscillations. KamLAND data have been studied in section 4, together with solar data.

## 6.1 Technical details

It is convenient to compute oscillation probabilities using the neutrino and anti-neutrino density matrices. We convert the initial value (e.g. $\rho(E_\nu) = \mathrm{diag}\,(\Phi_e(E_\nu), \Phi_\mu(E_\nu), 0, 0)$ for atmospheric neutrinos) to the instantaneous mass eigenstate basis, $\rho_m = V^\dagger \rho V$. In this basis evolution in each medium (air, mantle, core) is simply given by a diagonal matrix of phases, $\mathscr{U} = \mathrm{diag}\,\exp(-2i\delta)$ where $\delta_i = m^2_{\nu_{mi}} L/4E_\nu$. Using the matrix density in the mass eigenstate basis, we can analytically average 'fast' oscillations to their mean value by appropriately inserting a small imaginary part $\epsilon$ in the oscillation phases $\delta$. This is achieved by evolving the matrix density as $\rho^m_{ij}(L) = \rho^m_{ij}(0) e^{2i\delta_{ij} - \epsilon|\delta_{ij}|}$ where $\delta_{ij} = \delta_i - \delta_j$ and $\epsilon$ is an arbitrary positive small number (we choose $\epsilon = 0.01|\delta_{ij}|$). This makes computations much faster than usual techniques which require lengthy numerical averages of the oscillation factors. In the simplest case of vacuum oscillations of 2 neutrinos this amounts to modify the oscillation factor as $\sin^2\delta_{12} \to (1 - e^{-|\delta_{12}\epsilon|}\cos 2\delta_{12})/2$.

At the air/mantle and mantle/core boundaries eigenstates change in a non-adiabatic way: this effect is accounted by the 'level-crossing' flavour matrices $P$ already described at page 15.

Our fit of atmospheric data takes into account all most recent results: SK atmospheric data [71], the K2K spectrum and total rate [72], and MACRO [73] data about trough-going muons. These events arise from neutrino scatterings in the rock below the detector: MACRO is competitive with SK because the important parameter is the surface of the detector, rather than its mass. We do not include data from older atmospheric experiments, which studied essentially the same kind of observables better measured by SK. Data are fitted by forming a global $\chi^2$. Uncertainties are taken into account following [71], and systematically working in Gaussian approximation. More naïve definitions of the $\chi^2$ (e.g. fitting only the zenith-angle spectra of the single classes of events) do not give significantly different final results.

Atmospheric data contain the evidence for the atmospheric anomaly. We assume it is due to $\nu_\mu \to \nu_\tau$ oscillations and take into account the uncertainty on $\Delta m^2_{\mathrm{atm}}$ and on $\theta_{\mathrm{atm}}$ using the same technique developed in section 4.2 for marginalizing over $\Delta m^2_{\mathrm{sun}}$ and on $\theta_{\mathrm{sun}}$. Even in the atmospheric case, this technique now gives an accurate analytical approximation to the usual active-only atmospheric fit (not shown). As previously discussed, we assume $\theta_{13} = 0$.

Finally, we include $\bar{\nu}_e$ disappearance data from the CHOOZ [74] (14 bins) and BUGEY [75] (60 bins) reactor experiments. We include $\nu_\mu$ disappearance data from CDHS [76] (15 bins) and CCFR [77] (15 bins). NUTEV data could give additional information, if certain anomalous features will be understood [78]. Although disappearance experiments give the dominant constraint on sterile effects, we also include $\bar{\nu}_\mu \to \bar{\nu}_e$ data from KARMEN [79], using the likelihood computed by the KARMEN collaboration on an event-by-event basis.[24] LSND results are not included and separately discussed in section 6.4. Finally, we include NOMAD and CHORUS data on $\nu_\mu \to \nu_\tau$ [80], which are relevant in the case of $\nu_3/\nu_{\rm s}$ mixing at $\Delta m^2 \sim 10\,{\rm eV}^2$.

## 6.2 Results

Since there are many relevant experiments, it is useful to divide them into two classes, and separately study their impact:

1) Fig.s 11 show the constraints from experiments that are not sensitive to the atmospheric anomaly (CHOOZ, BUGEY, CDHS, CCFR, KARMEN, NOMAD, CHORUS). Sterile oscillation effects in such experiments are simply described by eq. (2), so that we only had to compile their results. Disappearance experiments provide the dominant constraints.

2) Atmospheric neutrinos are a powerful probe of neutrino oscillations with large mixing angle and $\Delta m^2 \gtrsim 10^{-4}\,{\rm eV}^2$. Fig.s 12 show how the experiments that see the atmospheric anomaly (SK, MACRO and K2K) constrain extra oscillations into sterile neutrinos.

Analyzing the second class of experiments requires a non trivial work: these experiments probe sterile mixing in a significant but indirect way.

The upper limit on the 'sterile fraction involved in atmospheric oscillations' conventionally quoted in the literature corresponds to the following 'minimal' configuration: $\nu_{\rm s}/\nu_\tau$ mixing with $\Delta m^2_{34} \gg \Delta m^2_{\rm atm}$. In this limit, the 'sterile fraction' is related to our $\theta_{\rm s}$ angle by $\eta_{\rm s} = \sin^2\theta_{\rm s}$ and our analysis reasonably agrees with previous computations. Atmospheric neutrinos oscillate at a single detectable frequency. Matter effects become relevant at higher neutrino energies and suppress active/sterile mixing without affecting $\nu_\mu \to \nu_\tau$ oscillations. This effect allows to indirectly discriminate the two channels. Sterile oscillations are mostly disfavoured by the zenith-angle spectra of $\mu$-like events with TeV-scale energies.

More general active/sterile oscillation schemes manifest in different ways. A sterile neutrino mixed with different flavours can give appearance signals. Active/sterile oscillations with $\Delta m^2$ comparable to $\Delta m^2_{\rm atm}$ give oscillations at multiple frequencies, distorted by matter effects. When $\Delta m^2_{34} < 0$ matter effects increase the oscillation length and give a non-standard energy and path-length dependence of $P(\nu_\mu \to \nu_\mu)$. SK can best probe such effects with its multi-GeV $\mu$-like sample. However, SK cannot safely test if an oscillation dip is present. This kind of studies needs a dedicated future detector [81].

The SK collaboration probes sterile effects in another more direct way: selecting a sample of NC-enriched events [71]. In absence of a precise description of the cuts performed to obtain the NC-enrichment, we have not included this sample (as also done in previous reanalyses of SK data). The 'minimal' active/sterile configuration is more strongly constrained indirectly by the

[24] We thank K. Eitel and M. Steidl for giving us the table of the KARMEN likelihood, and B. Louis and G. Mills for the LSND likelihood.

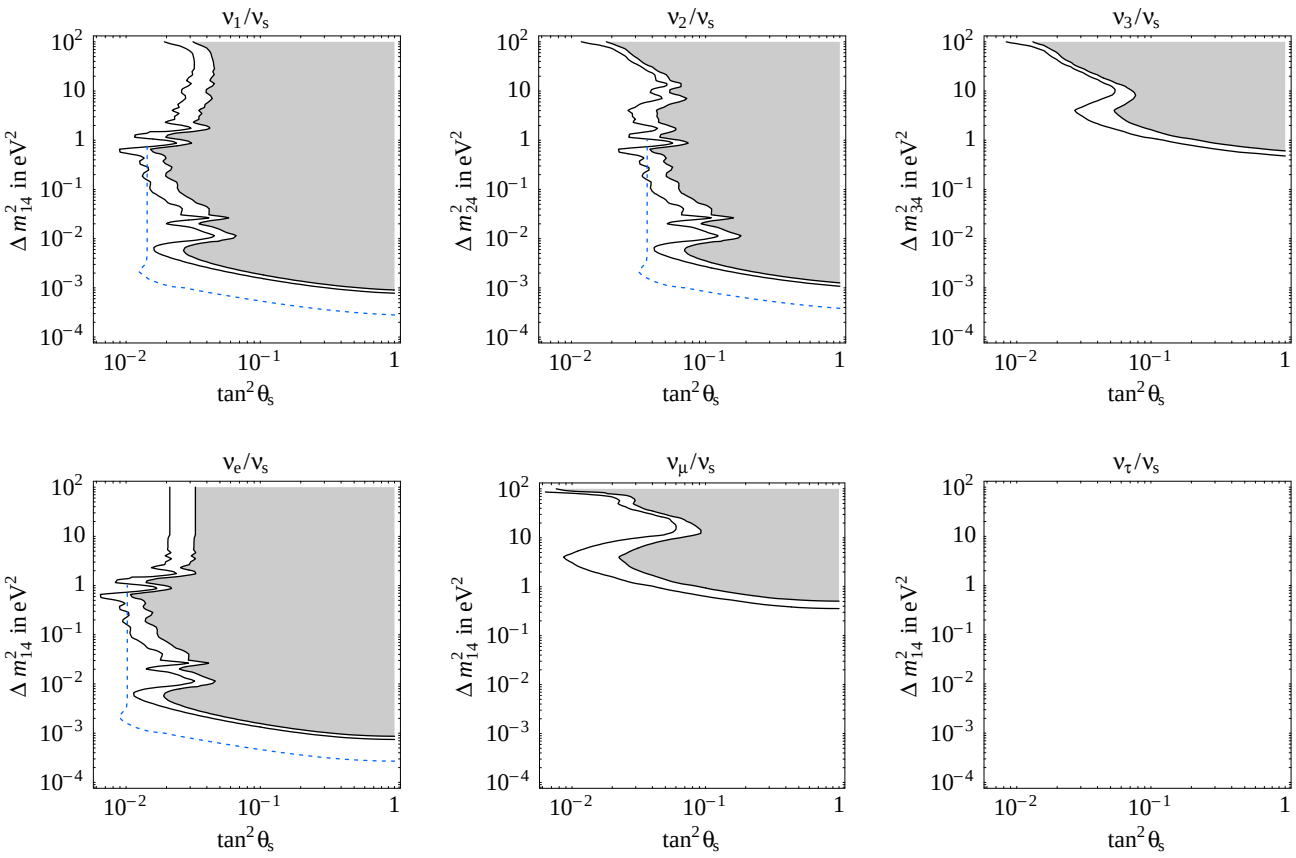


Figure 11: **Sterile mixing: effects in short base-line experiments** CHOOZ, BUGEY, CDHS, CCFR, KARMEN, NOMAD, CHORUS. *Shaded regions: excluded at* $90, 99\%$ *C.L. The blue dashed lines estimate the region that seems explorable by a future short-baseline reactor experiment. The plot is symmetric under* $\tan\theta_s \leftrightarrow 1/\tan\theta_s$ *so that we only show* $\tan\theta_s \leq 1$.

zenith-angle spectra. We estimate that this remains true in most of the parameter space, and consequently we do not include in our final results our approximate reanalysis of NC-enriched data.

As in the solar case, we looked if present data contain some evidence for sterile effects which correct in a minor way many observables, by searching for local minima of the global $\chi^2$. No statistically significant hint is found: since subleading sterile effects do not improve the global fit in a significant way (at most by $\Delta\chi^2 \approx 4$) our plots only show excluded regions. The excluded region in fig.s 12d, e (which correspond to $\nu_\mu/\nu_s$ and to $\nu_\tau/\nu_s$ mixing) extends down to $\Delta m^2_{41} = 0$ because even in this limit there are sterile oscillations at the atmospheric and solar frequencies.

It is useful to compare the sensitivity of the two classes of experiments, 1) and 2). Since there are no MSW resonances, all these experiments are sensitive only to relatively large sterile mixing, $\theta_s \gtrsim 0.1$. Sterile mixing with $\nu_e$ (and with the $\nu_1$ and $\nu_2$ mass eigenstates that contain a sizable $\nu_e$ fraction) is better probed by reactor experiments, although $e$-like events at SK extend the sensitivity down to smaller values of $\Delta m^2$. On the contrary atmospheric experiments give more stringent tests of $\nu_s/\nu_\tau$ mixing and of $\nu_s/\nu_\mu$ mixing. Within standard cosmology, the

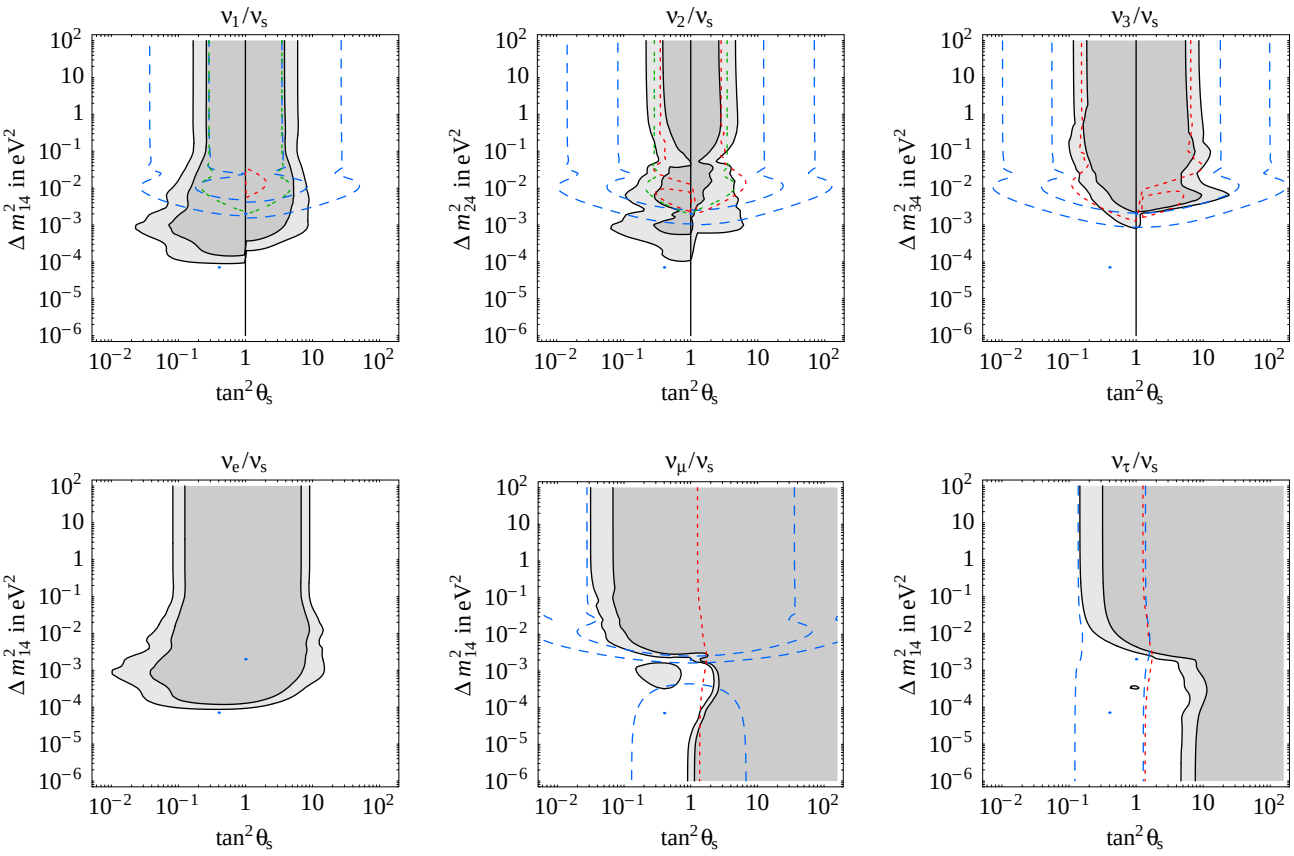


Figure 12: **Sterile mixing: effects in atmospheric neutrinos (SK, MACRO) and K2K.** *No statistically significant evidence is found. Shaded regions: excluded at* $90, 99\%$ *C.L. Coloured lines are iso-curves of a few promising signals. Blue dashed lines:* $5\%$ *and* $1\%$ *reduction of the NC rate at MINOS. Green dot-dashed lines:* $P_{e\mu} = 0.01$. *Red dotted lines:* $|\Delta P_{\mu\tau}| = 0.01$ *at CNGS.*

sterile effects detectable by the experiments discussed in this section are already disfavoured by measurements of the primordial $^4$He abundancy, and can be fully tested by future CMB or BBN data.

A detailed analysis of capabilities of future beam or reactor neutrinos as probes of sterile neutrinos seems not necessary. In fact, there are many proposals motivated by other considerations, and in each case it is easy to compute sterile effects. We only make a few general comments.

The blue dashed line in fig.s 11 shows what can achieved by a future high-precision short-baseline reactor experiment able of detecting a 2% deficit in the $\bar{\nu}_e$ flux [82]. Sterile oscillations give a $\bar{\nu}_e$ deficit, which might be energy-dependent if the sterile oscillation length at $E_\nu \sim$ few MeV is comparable to the base-line $L$. Both are unknown; we assumed $L \sim 2\,\text{km}$. Most of the explorable region at small $\Delta m^2$ is already excluded by solar and atmospheric experiments. The region with large $\Delta m^2 \sim \text{eV}^2$ is more difficult because even a near detector only sees averaged oscillations; one has to rely on theoretical predictions for the total flux of reactor $\bar{\nu}_e$ [83].

Sterile oscillations with large $\Delta m^2 \sim \text{eV}^2$ have a wave-length comparable to the earth radius at energies $E_\nu \sim$ TeV: experiments such as AUGER and IceCube can study atmospheric neutrinos in this energy range, and could see an anomalous zenith-angle dependence if $\theta_{\rm s}$ is large enough [84].

Future atmospheric experiment such as Monolith [81] could test if the first oscillation dip is present as predicted by $\nu_\mu \to \nu_\tau$ oscillations. Sterile effects with $\Delta m^2 \sim \Delta m^2_{\rm atm}$ can significantly distort the expected oscillation pattern.

Distortions not related to earth matter effects can also be searched by the planned $\nu_\mu$-beam experiments. Furthermore, the MINOS detector can statistically distinguish NC/CC events that are tagged as short/ long tracks, and it should be possible to measure the NC rate with 5% precision [85]. The blue dashed lines in fig.s 12 correspond to a 5% and 1% anomaly in the NC total rate in a $\nu_\mu$ beam experiment with $L = 730\,\text{km}$ and Minos-like parent energy spectrum.

A sterile neutrino can also manifest as $\nu_\tau$ appearance: considering a CNGS-like beam [86] in fig.s 12 we show iso-curves corresponding to an average $\nu_\mu \to \nu_\tau$ conversion probability $\pm 0.01$ different from atmospheric oscillations only (which give a conversion probability of about 0.02, depending on the precise value of $\Delta m^2_{\rm atm}$ and on the average energy of the beam).

Constraints from reactor experiments make more difficult, but not impossible, to have detectable $\nu_e$ appearance in a $\nu_\mu$ beam (or $\nu_\mu$ appearance in a $\nu_e$ beam) as signals of active/sterile oscillations. In experiments sensitive to atmospheric oscillations a non zero $\theta_{13}$ gives such effects. Assuming $\theta_{13} = 0$, in fig. 12 we show iso-curves corresponding to a $\nu_\mu \to \nu_e$ conversion probability of 0.01.

## 6.3 Hints and anomalies

To conclude, we list some possibly anomalous features of present data:

- The total rate of $e$-like events at SK is higher than the expected central value. The $\mu/e$ ratio seems to be too low (see e.g. [87]). Constraints from solar, atmospheric and short-baseline data show that sterile neutrinos can reduce the $\mu$ rate (e.g. in the case of $\nu_\mu/\nu_{\rm s}$ mixing with $\Delta m^2_{14} \sim 10^{-4}\,\text{eV}^2$) but cannot increase the $e$ rate.

- The total rate of trough-going muons at SK is higher than the expected central value. Predictions and direct measurements of cosmic ray primaries at the relevant energies are difficult [88].

- The LSND result [4], discussed below.

## 6.4 LSND

The LSND experiment [4] finds an evidence for $\bar\nu_\mu \to \bar\nu_e$, that ranges between 3 to $7\sigma$ depending on how data are analyzed. It is difficult to conceive new physics that can explain the LSND result compatibly with all other constraints. Among reasonably conservative interpretations, a sterile neutrino with eV-scale mass seems to be the less disfavoured possibility [89, 52, 6]. According to this interpretation the LSND anomaly arises as $\nu_\mu \to \nu_{\rm s} \to \nu_e$ so that the effective

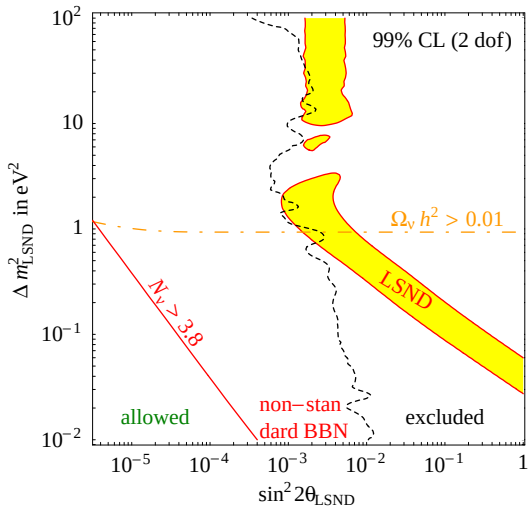


Figure 13: **The LSND anomaly interpreted as oscillations of 3+1 neutrinos**. *Shaded region: suggested at 99% C.L. by LSND. Black dotted line: 99% C.L. global constraint from other neutrino experiments (mainly Karmen, Bugey, SK, CDHS). Continuos red line:* $N_\nu = 3.8$ *thermalized neutrinos. Dot-dashed orange line:* $\Omega_\nu h^2 = 0.01$.

$\theta_{\rm LSND}$ $\nu_\mu/\nu_e$ mixing angle is predicted to be $\theta_{\rm LSND} \approx \theta_{es} \cdot \theta_{\mu s}$. This formula is valid only for small mixing angles, and eq. (2) gives the general expression. This prediction gives rise to 3 problems:

1) $\nu_e$ and $\nu_\mu$ disappearance experiments imply that $\theta_{es}$ are $\theta_{\mu s}$ are somewhat smaller than what suggested by LSND [89, 52, 6];

2) standard BBN predicts that the sterile neutrino thermalizes, so that primordial abundances should have values corresponding to $N_\nu = 4$ [90];

3) according to standard cosmology, the sterile neutrino gives a contribution to the neutrino density $\Omega_\nu$ somewhat larger than what suggested by global fit of CMB and LSS data (see e.g. [91]).

Concerning points 2) and 3), there is not yet general consensus that the sterile neutrino thermalizes, maybe because this LSND issue has never been analyzed by authors that performed, at the same time, a precise study of neutrino data and of cosmology with mixed neutrinos. Estimates indicate that the region favoured by LSND lies well inside the region where the sterile neutrino is thermalized [90]. This is confirmed by our analysis, shown in fig. 13. In the relevant region the constraint on $\Omega_\nu$ is well approximated by the horizontal line corresponding to $\Omega_\nu h^2 = m_4/93.5\,\text{eV}$, as assumed in previous analyses [91, 6]. The accurately computed constraint starts to be weaker only at much smaller values of the effective $\theta_{\rm LSND}$ mixing angle.

In fig. 13 the BBN constraint has been minimized (when allowed by neutrino data) setting $\theta_{es} \approx \theta_{\mu s} \approx \theta^{1/2}_{\rm LSND}$. We see that short-baseline experiments sensible to a $P(\nu_\mu \to \nu_e)$ about 2 orders of magnitude smaller than the value suggested by LSND are needed to probe regions compatible with standard BBN.

# 7 Summary

A few years ago active/sterile oscillations were studied as an alternative to active/active oscillations. For example, it was shown that neither the solar nor the atmospheric anomaly can be produced by oscillations into sterile neutrinos compatibly with standard BBN. These active vs sterile issues have now been firmly solved by experiments, and the new relevant questions become:

> How large can be the subdominant sterile component possibly present in solar or atmospheric oscillations? How can we discover new anomalies due to sterile effects?

In order to address these issues we systematically compared oscillation effects generated by one sterile neutrino (including the effects of the now established solar and atmospheric oscillations) with present experiments and studied capabilities of future probes, extending previous analyses in several ways. Almost all previous analyses that studied these new questions considered only the peculiar sterile oscillation pattern that gives the simplest physics: the sterile neutrino mixes with a specific flavour ($\nu_{\mu,\tau}$ in solar analyses, $\nu_\tau$ in atmospheric ones) and has a large mass, $\Delta m^2 \gg \Delta m^2_{\rm atm,sun}$. Dropping each one of these assumptions gives quite different physics. We explored the whole parameter space (three sterile mixing parameters and one sterile mass) producing precise results for six representative slices, that span the spectrum of the various possibilities. We considered one extra sterile neutrino with arbitrary mass $m_4$, and allowed it to mix with

$$\nu_e \quad \text{or} \quad \nu_\mu \quad \text{or} \quad \nu_\tau \quad \text{or} \quad \nu_1 \quad \text{or} \quad \nu_2 \quad \text{or} \quad \nu_3$$

where $\nu_{1,2,3}$ are the mass eigenstates in absence of sterile mixing. The spectrum of active neutrinos is not yet fully known: rather than studying all possible cases we focussed on what we believe is most plausible case: we assumed normal hierarchy of active neutrinos (i.e. $m_1 \ll m_2 \approx m_3/6$) and that $\theta_{13}$ is small enough that we can neglect its effects. If experiments will contradict these assumptions, it will be easy to update our results; most of them do not depend on these assumptions.

We considered the most promising ways to probe the existence of eV-scale sterile neutrinos. Most probes are based on a careful study of natural sources of neutrinos (the universe, the sun, supernovæ, cosmic rays,...) which have their own peculiar capabilities and limitations. We studied how one extra sterile neutrino affects BBN (helium-4, deuterium), CMB, LSS and solar, atmospheric, reactor, beam experiments. The sensitivity of some of these probes is enhanced by MSW resonances [23]. In cosmology, active $\nu$ and $\bar\nu$ encounter a MSW resonance with sterile neutrinos lighter than active ones. Roughly the same happens to supernova $\bar\nu_e$ (that also experience less important MSW resonances in the opposite situation). On the contrary, solar $\nu_e$ encounter a MSW resonance with sterile neutrinos heavier than active ones.

Fig.s 14 combines present constraints. Each probe is described in greater detail in its specific series of figures: fig.s 3 for cosmology, fig.s 6 for solar experiments, fig.s 9 for supernovæ, fig.s 11 for short base-line experiments, fig.s 12 for atmospheric experiments. These figures also show the capabilities of some future experiments, that we now try to summarize in words.

- Compatibility with standard BBN constrains sterile oscillations occurred at temperatures $T \gtrsim 0.1\,\text{MeV}$. It is very important to improve measurements of the **helium-4** primordial

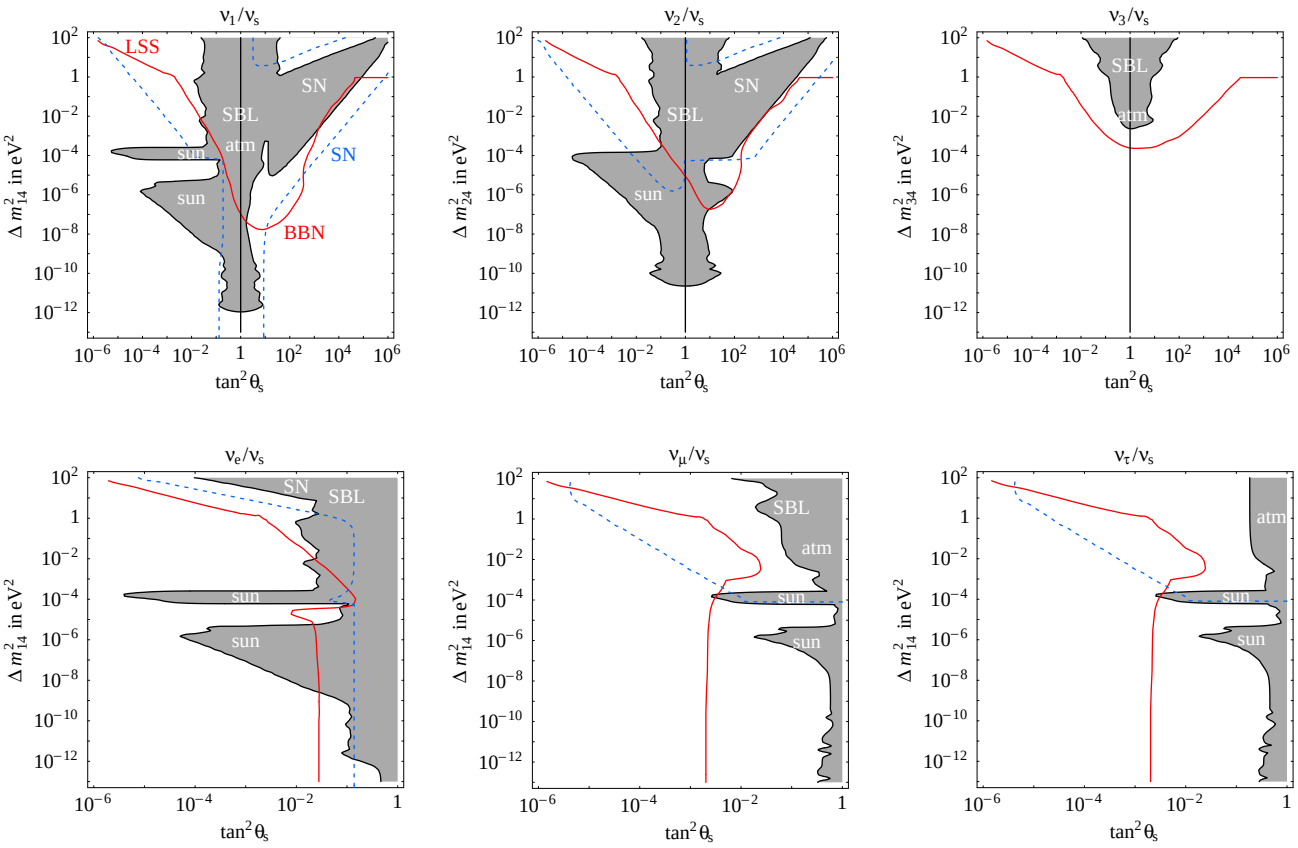


Figure 14: **Summary of sterile neutrino effects**. *The shaded region is excluded at* 99% *C.L. (2 dof) by solar or atmospheric or reactor or short base-line experiments. We shaded as excluded also regions where sterile neutrinos suppress the SN1987A* $\bar{\nu}_e$ *rate by more than* 70%. *This rate is suppressed by more than* 20% *inside the dashed blue line, that can be explored at the next SN explosion if it will be possible to understand the collapse well enough. Within standard cosmology, the region above the red continuous line is disfavoured (maybe already excluded) by BBN and LSS. Plots in the various sections show how much each probe can be improved by future experiments.*

abundancy (that we parameterize in terms of an effective number of neutrinos $N_\nu^{^4\mathrm{He}}$, see eq. (4)) until $N_\nu^{^4\mathrm{He}} = 4$ will be safely tested. This requires overcoming 'systematic' uncertainties. The helium-4 abundancy is sensitive to two different sterile effects: increase of the total neutrino density, and depletion of electron-neutrinos. The second effect makes $N_\nu^{^4\mathrm{He}}$ sensitive to sterile oscillations down to $\Delta m^2 \sim 10^{-8}\,\mathrm{eV}^2$, while the first effect becomes negligible at $\Delta m^2 \lesssim 10^{-5}\,\mathrm{eV}^2$.

However, if BBN were non-standard, a modified density of electron neutrinos could compensate the sterile corrections to $N_\nu^{^4\mathrm{He}}$: for example helium-4 constraints on sterile oscillations can be evaded by allowing a large neutrino asymmetry.

- For all these reasons it is important to measure a second BBN effect. The **deuterium** primordial abundancy is affected by milder systematic problems: in the future it might be possible to improve its measurement obtaining an uncertainty on the effective parameter $N_\nu^{\mathrm{D}}$ (precisely defined in eq. (4))) significantly below 1, possibly making deuterium the most significant BBN probe. We have computed the ranges of active/sterile oscillation parameters that significantly affect $N_\nu^{\mathrm{D}}$: it is less sensitive than helium-4 to $\nu_e$ depletion and therefore to values of $\Delta m^2$ below $10^{-5}\,\mathrm{eV}^2$ (fig. 3).

- Future studies of **Cosmic Microwave Background** acoustic oscillations should allow to precisely measure the total neutrino density $N_\nu^{\mathrm{CMB}}$ at recombination ($T \sim$ eV) with $\pm 0.2$ (Planck) or maybe $\pm 0.05$ (CMBpol) error [17]. Neutrinos affect CMB in various ways; neutrino free-streaming offers a clean signature that allows to count neutrinos. Sterile neutrinos affect $N_\nu^{\mathrm{CMB}}$ only if $\Delta m^2 \gtrsim 10^{-5}\,\mathrm{eV}^2$; in such a case $N_\nu^{\mathrm{CMB}} \approx N_\nu^{^4\mathrm{He}} \approx N_\nu^{\mathrm{D}}$. Therefore CMB will cover only a part of the region that BBN could probe with fully reliable measurements of the helium-4 or deuterium abundances.

- CMB also allows to probe eV-scale $\nu$ masses. Smaller $\nu$ masses can be probed by measuring how much galaxies are clustered, because neutrinos become non relativistic when the observable universe had a size comparable to present cluster of galaxies. Relativistic neutrinos freely move and tend to reduce the amount of clustering. Recently, **Large Scale Structure** data (together with precise CMB measurements) gave a bound on the present energy density in neutrinos $\Omega_\nu < 0.0076$ at 95 % C.L. [8, 19], dominated by neutrino masses (rather than neutrino energy). With only active neutrinos this implies a significant bound on their mass, $m_\nu < 0.23\,\mathrm{eV}$ [8, 19].

  Sterile neutrinos contribute to $\Omega_\nu$ (a small non-thermal population of relatively heavy sterile neutrinos also modifies the way $\Omega_\nu$ manifests). For small active/sterile mixing LSS constrains sterile oscillations more strongly than BBN (fig. 3).

- **Solar** $\nu_e$ experiments have explored sterile oscillations not testable by BBN, thanks to two different effects. (1) MSW resonances make solar $\nu_e$ sensitive to small active/sterile mixing and $\Delta m^2 \gtrsim 10^{-8}\,\mathrm{eV}^2$. (2) With large mixing, solar $\nu_e$ are sensitive down to $\Delta m^2 \sim 10^{-12}\,\mathrm{eV}^2$. Future experiments will explore new aspects of the solar neutrino anomaly, allowing to measure in a redundant way the active oscillation parameters or to discover a new anomaly. We emphasize one qualitative point. Due to LMA oscillations, neutrinos exit from the sun as almost pure $\nu_2$ at energies $E_\nu \gtrsim$ few MeV. Neutrinos with these

energies have been precisely studied by SK and SNO, but are almost unaffected by sterile oscillations if they involve mostly $\nu_1$. This could happen either when $\nu_s$ mixes with $\nu_1$, or when $\nu_s$ experiences a level-crossing with $\nu_1$. Therefore *there is a whole class of sterile effects which manifest only at* $E_\nu \lesssim$ few MeV — an energy range explored so far only by Gallium experiments. Future precise measurement of solar $\nu_e$ at sub-MeV energies will allow to significantly extend searches for active/sterile effects. Part of these extended region can be soon tested by Borexino, where a sterile neutrino can manifest as day/night variations, or as seasonal variations, or even by reducing the total rate.

- **Supernova** neutrinos will be good probes of sterile oscillations because have a different pattern of MSW resonances and a longer base-line than solar $\nu_e$. Consequently supernova $\bar{\nu}_e$ are more sensitive than solar $\nu_e$ in two main cases: (a) small $\Delta m^2 \gtrsim 10^{-18}\,\mathrm{eV}^2$ with large $\theta_s$; (b) $\nu_s$ lighter than $\nu_1$ with small mixing. Oscillations into one sterile neutrino can reduce the $\bar{\nu}_e$ rate by up to 80% (see fig.s 9) and, in a more restricted range of oscillation parameters, vary the average $\bar{\nu}_e$ energy by 30%. SN1987A data agreed with expectations. Future SN experiments can perform quantitative test, but it is not clear how to deal with theoretical uncertainties. We also discussed other less promising astrophysical probes.

- **Atmospheric** experiments (SK, MACRO, K2K) indirectly exclude active/sterile oscillations with $\Delta m^2 \gtrsim 10^{-3\div 4}\,\mathrm{eV}^2$ and $\tan^2\theta_s \gtrsim 0.1 \div 0.2$. Up to minor differences, this applies to all flavours (fig. 12). **Terrestrial experiments** that mainly probed disappearance of $\bar{\nu}_e$ and $\nu_\mu$ (CHOOZ, CDHS,...) exclude active/sterile mixings with these flavours with $\tan^2\theta_s \gtrsim 0.03$ and $\Delta m^2 \gtrsim 10^{-3}\,\mathrm{eV}^2$ (fig. 11). Therefore future short-baseline experiments can search for sterile effects with smaller $\theta_s$. Possible signals are $\bar{\nu}_e$ disappearance in reactor experiments, a deficit of NC events or $\nu_\tau$ appearance in beam experiments. Within standard cosmology these effects can be probed by CMB and BBN, which already disfavour them.

We listed present anomalies that can be interpreted as due to sterile neutrinos. None looks particularly significant, with the possible exception of the LSND anomaly, that can be due to oscillations of '3 + 1' neutrinos. Our precise study confirms that the extra sterile neutrino suggested by LSND thermalizes almost completely before BBN (in agreement with estimations of most previous analyses). In fig. 13 we plot, as function of the effective LSND oscillation parameters $\theta_{\mathrm{LSND}}$ and $\Delta m^2_{\mathrm{LSND}}$, the constraints on $N_\nu^{^4\mathrm{He}} \simeq N_\nu^{\mathrm{D}} \simeq N_\nu^{\mathrm{CMB}}$ (mainly from helium-4 data) and $\Omega_\nu$ (mainly from LSS data): in the relevant region our precise plot negligibly differs from previous estimates [91, 6]. The 3+1 interpretation of LSND is not compatible with standard BBN, and gives a $\Omega_\nu$ which is only marginally compatible with standard cosmology.

**Acknowledgments** We thank S. Woosley, A. Burrows, P. Di Bari, S. Sarkar, S. Pascoli, A. Romanino, K. Olive. The work of M.C. is supported in part by the USA department of energy under contract DE-FG02-92ER-40704. Part of the work of M.C. was done while at scuola normale superiore (Pisa). The authors thank the CERN theory division, where part of the work was done.

# References


[1] For an old but still useful review see R.V. Wagoner, W.A. Fowler, F. Hoyle, *The Astrophys. J.* 148 (1967) 3. For a recent review see S. Sarkar, *Rept. Prog. Phys.* 59 (1996) 1493 (*hep-ph/9602260*). For precision computations, see D.A. Dicus et al., *Phys. Rev.* D26 (1982) 2694. R.E. Lopez, M.S. Turner, *Phys. Rev.* D59 (1999) 103502 (*astro-ph/9807279*). S. Esposito et al., *Nucl. Phys.* B568 (421) 2000. A. Cuoco et al., *astro-ph/0307213*.

[2] A. Bandyopadhyay et al., *hep-ph/0309174*. T. Schwetz, *hep-ph/0311217*.

[3] See e.g. the talk by K. Okumura at the NO-VE workshop, Venice 3–5 dec. 2003, available at the web page axpd24.pd.infn.it/NO-VE/NO-VE.html.

[4] The LSND collaboration, *hep-ex/0104049*.

[5] V. Berezinsky et al., as cited in [7].

[6] A. Strumia, *Phys. Lett.* B539 (2002) 91 (*hep-ph/0201134*). Other authors finally agree that '2+2' oscillations are no longer viable, see e.g. M. Maltoni, T. Schwetz, M.A. Tortola, J.W.F. Valle, *Nucl. Phys.* B643 (2002) 321 (*hep-ph/0207157*). However some controversy remains, see e.g. R. Foot, *Phys. Lett.* B496 (2000) 169 (*hep-ph/0007065*), R. Foot, *Mod. Phys. Lett.* A18 (2003) 207 (*hep-ph/0210393*) and H. Päs, L.G. Song, T. J. Weiler, *Phys. Rev.* D67 (2003) 073019 (*hep-ph/0209373*). According to R. Foot, *hep-ph/0303005*. the NC-enriched sample of SK atmospheric data might be less enriched than what claimed by SK. The K2K near detector is measuring the relevant cross sections, with results reported by S. Nakayama at the NuInt04 conference (web site: nuint04.lngs.infn.it).

In any case, exclusion of '2+2' oscillations follows from global fits, not directly from a few simple measurements.

[7] Models with sterile neutrinos. Light fermions from a discrete symmetry: E. Ma, P. Roy, *Phys. Rev.* D52 (1995) 4780. From a continuos symmetry: E. Ma, *Mod. Phys. Lett.* A11 (1996) 1893. From a supersymmetric $R$-symmetry: E.J. Chun, A.S. Joshipura, A.Yu. Smirnov, *Phys. Lett.* B357 (1995) 608. As Goldstone particles: E.J. Chun, A.S. Joshipura, A.Yu. Smirnov, *Phys. Rev.* D54 (1996) 4654. As modulinos: K. Benakli, A.Yu. Smirnov, *Phys. Rev. Lett.* 79 (1997) 4314. From a mirror world: S.I. Blinikov, M. Yu Khlopov, *Sov. Astron.* 27 (1983) 371. Z. Silagadze, *Phys. Atom. Nucl.* 60 (1997) 272 (*hep-ph/9503481*). R. Foot, R. Volkas, *Phys. Rev.* D52 (1995) 6595 (*hep-ph/9505359*). Z.G. Berezhiani, R.N. Mohapatra, *Phys. Rev.* D52 (1995) 6607 (*hep-ph/9505385*). V. Berezinsky, M. Narayan, F. Vissani, *hep-ph/0210204*. From compositness: N. Arkani-Hamed, Y. Grossman, *hep-ph/9806223*. From warped extra dimensions or compositness: T. Gherghetta, *hep-ph/0312392*. From mirror fermions: M. Bando, K. Yoshioka, *Prog. Theor. Phys.* 100 (1998) 1239 (*hep-ph/9806400*). From supersymmetry breaking: K.S. Babu, T. Yanagida, *Phys. Lett.* B491 (2000) 148 (*hep-ph/0008110*). F. Borzumati, K. Hamaguchi, T. Yanagida, *Phys. Lett.* B497 (2001) 259 (*hep-ph/0011141*). Small sterile masses from supersymmetric flat directions: P. Langacker, *Phys. Rev.* D58 (1998) 093017 (*hep-ph/9805281*). Models with 2 sterile neutrinos: K.S. Babu, G. Seidl, *hep-ph/0312285*. K.L. McDonald, B.H.J. McKellar, A. Mastrano, *hep-ph/0401241*. W. Krolikowski, *hep-ph/0402183*.

[8] C.L. Bennett et al., *astro-ph/0302207* and D.N. Spergel et al., *astro-ph/0302209*.

[9] Recent measurements of the helium-4 primordial abundancy. Y.I. Izotov, T.X. Thuan, *Astrophys. J.* 500 (1998) 188. K.A. Olive, E. Skillman, G. Steigman, *Astrophys. J.* 483 (1997) 788. Y.I. Izotov, F.H. Chaffee, C.B. Foltz, R.F. Green, N.G. Guseva. T.X. Thuan, *Astrophys. J.* 527 (1999) 757. T.X. Thuan, Y.I. Izotov, *astro-ph/0003234*. M. Peimbert, A. Peimbert, M. T. Ruiz, *Astrophys. J.* 541 (2000) 688. A. Peimbert, M. Peimbert, V. Luridiana, *Astrophys. J.* 565 (2002) 668. Y.I. Izotov, T.X. Thuan, *astro-ph/0310421*. K.A. Olive, E.D. Skillman, *astro-ph/0405588*.

[10] P. Di Bari, *Phys. Rev. D* 65 (2002) 043509 and addendum: P. Di Bari, *Phys. Rev. D* 67 (2003) 127301; R. H. Cyburt, B. D. Fields, K. A. Olive, *Phys. Lett. B* 567 (2003) 227; S. Hannestad as cited in [19]; V. Barger et al., *hep-ph/0305075*; K.N. Abazajian, *Astropart. Phys.* 19 (2003) 303 (*astro-ph/0205238*).

[11] Recent measurements of the deuterium primordial abundancy. D. Kirkman, D. Tytler, S. Burles, D. Lubin, J.M. O'Meara, *Astrophys. J.* 529 (2000) 665. J. M. O'Meara, D. Tytler, D. Kirkman, N. Suzuki, J.X. Prochaska, D. Lubin, A.M. Wolfe, *Astrophys. J.* 552 (2001) 718. D. Kirkman, D. Tytler, N. Suzuki, J.M. O'Meara, D. Lubin, *astro-ph/0302006*. M. Pettini, D.V. Bowen, *Astrophys. J.* 560 (2001) 41. S. D'Odorico, M. Dessauges-Zavadsky, P. Molaro, *Astronomy and*

*Astrophysics* 368 (2001) L21. S.A. Levshakov, P. Molaro, M. Dessauges-Zavadsky, S. D'Odorico, *Astrophys. J.* 565 (2002) 696.

[12] F.L. Villante, A.D. Dolgov, *hep-ph/0310138*.

[13] A. Strumia, F. Vissani, a full review on neutrino masses and mixings, IFUP-TH/2004-01, hopefully to appear.

[14] Sterile/active oscillations and BBN: D. Kirilova, Dubna preprint JINR E2-88-301. R. Barbieri, A. Dolgov, *Phys. Lett.* B237 (1990) 440. K. Enqvist et al., *Phys. Lett.* B249 (1990) 531. K. Kainulainen, *Phys. Lett.* B244 (1990) 191. R. Barbieri, A. Dolgov, *Nucl. Phys.* B349 (1991) 743. K. Enqvist et al., *Nucl. Phys.* B373 (1992) 498. J.M. Cline, *Phys. Rev. Lett.* 68 (1992) 3137. X. Shi, D.N. Schramm, B.D. Fields, *Phys. Rev.* D48 (1993) 2563. R. Foot, M.J. Thomson, R.R. Volkas, *Phys. Rev.* D53 (1996) 5349. E. Lisi, S. Sarkar, F.L. Villante, *Phys. Rev.* D59 (1999) 123520 (*hep-ph/9901404*). D.P. Kirilova, M.V. Chizhov, *Phys. Rev.* D58 (1998) 073004 (*hep-ph/9707282*). D.P. Kirilova, M.V. Chizhov, *Nucl. Phys.* B591 (2000) 457 (*hep-ph/9909408*). A.D. Dolgov et al., *Nucl. Phys.* B632 (2002) 363. H.N. Abazajian, *astro-ph/0205238*.

[15] R. Foot, R.R. Volkas, *Phys. Rev. Lett.* 75 (1995) 4350 (*hep-ph/9508275*).

[16] The rising of a large neutrino asymmetry (in specific regions of the parameters space) and its effects (for specific mixing patterns) are discussed e.g. in R. Foot, M.J. Thomson, R.R. Volkas, *Phys. Rev.* D53 (1996) 5349 (*hep-ph/9509325*), R. Foot and R.R. Volkas, *Phys. Rev.* D56 (1997) 6653 (*hep-ph/9706242*) and Erratum *ibid.* D59 (1999) 029901, N. F. Bell, R. Foot and R.R. Volkas, *Phys. Rev.* D58 (1998) 105010 (*hep-ph/9805259*), and also debated in A.D. Dolgov, S.H. Hansen, S. Pastor, D.V. Semikoz, *Astropart. Phys.* 14 (2000) 79 (*hep-ph/9910444*), P. Di Bari, R. Foot, R.R. Volkas, Y.Y.Y. Wong, *Astropart. Phys.* 15 (2001) 391 (*hep-ph/0008245*), D.P. Kirilova, M.V. Chizhov, *Nucl. Phys.* B591 (2000) 457 (*hep-ph/9909408*). The role of a primordial, non-dynamical neutrino asymmetry is also addressed in several papers of [10] and e.g. in V. Barger et al., *Phys. Lett.* B569 (2003) 123 (*hep-ph/0306061*).

[17] For a useful review see S. Bashinsky, U. Seljak, *astro-ph/0310198*.

[18] P. Crotty, J. Lesgourges, S. Pastor, *astro-ph/0302337*; E. Pierpaoli, *Mon. Not. Roy. Astron. Soc.* 342 (2003) L63; V. Barger, J. P. Kneller, H. S. Lee, D. Marfatia, G. Steigman, *Phys. Lett. B* 566 (2003) 8; S. Hannestad as cited in [19].

[19] The cosmological bound on neutrino masses is obtained by combining WMAP data with large-scale structure (and possibly other) data, see the papers in [8] and references therein. This is similar to pre-WMAP analyses, e.g. A. Lewis, S. Bridle, *Phys. Rev.* D66 (2002) 103511. Other (sometimes more conservative) analysis find similar (sometimes weaker) bounds: S. Hannestad, *JCAP* 0305 (2003) 004 (*astro-ph/0303076*), S.W. Allen, R.W. Schmidt, S.L. Bridle, *Mon. Not. Roy. Astron. Soc.* 346 (2003) 593 (*astro-ph/0306386*), M. Tegmark et al. [SDSS Collaboration], *Phys. Rev.* D69 (2004) 103501 (*astro-ph/0310723*) V.Barger et al., *Phys. Lett.* B595 (2004) 55 (*hep-ph/0312065*), P. Crotty, J. Lesgourgues, S. Pastor, *Phys. Rev.* D69 (2004) 123007 (*hep-ph/0402049*), U. Seljak et al., *astro-ph/0407372*. The robustness of the bound in presence of non-adiabatic incoherent fluctuations was studied in R.H. Brandenberger, A. Mazumdar, M. Yamaguchi, *Phys. Rev.* D69 (2004) 081301 (*hep-ph/0401239*).

[20] S. Hannestad, G. Raffelt, *hep-ph/0312154*. P. Crotty et al., *hep-ph/0402049*.

[21] Neutrino oscillations in the early universe. A. Dolgov, *Sov. J. Nucl. Phys.* 33 (1981) 700. L. Stodolsky, *Phys. Rev.* D36 (1987) 2273. A. Manohar, *Phys. Lett.* B186 (1987) 370. M.J. Thomson, B.H.J. McKellar, *Phys. Lett.* B259 (1991) 113. J. Pantaleone, *Phys. Lett.* B287 (1992) 128. A. Friedland, C. Lunardini, *hep-ph/0304055*. The formalism is clearly summarized in G. Sigl, G. Raffelt, *Nucl. Phys.* B406 (1993) 423. The dominant contribution to the refraction index was discussed in D. Nötzold, G. Raffelt, *Nucl. Phys.* B307 (1988) 924.

[22] A.D. Dolgov, *Phys. Rept.* 370 (2002) 333 (*hep-ph/0202122*).

[23] L. Wolfenstein, *Phys. Rev.* D17 (1978) 2369; S.P. Mikheyev, A. Yu Smirnov, *Sovietic Journal Nucl. Phys.* 42 (1986) 913.

[24] J. Bernstein et al., *Rev. Mod. Phys.* 61 (1989) 25. The paper R. Esmailzadeh, G.D. Starkman, S. Dimopoulos, *Astrophysical Journal* 378 (1991) 504, *'Primordial nucleosynthesis without a computer'*, contains rough analytical estimates. With a computer their methods can be used to develop accurate approximations that do not involve the slow integration of the network of Boltzmann BBN equations.

[25] A.D. Dolgov, F.L. Villante, *hep-ph/0308083*.

[26] S.W. Allen et al., as cited in [19]. See however S. Hannestad, *hep-ph/0312122* and SDSS collaboration as cited in [19].

[27] S.H. Hansen, Z. Haiman, *hep-ph/0305126*.

[28] C. Picciotto, M. Pospelov, *hep-ph/0402178*.

[29] A.M. Dziewonski, D.L. Anderson, *Phys. Earth Planet. Interior* 25 (1981) 297.

[30] Neutrino propagation in a varying density. S. Parke, *Phys. Rev. Lett.* 57 (1986) 1275. P. Pizzochero, *Phys. Rev.* D36 (1987) 2293. S.T. Petcov, *Phys. Lett.* B200 (1988) 373. T.K. Kuo, J. Pantaleone, *Phys. Rev.* D39 (1989) 1930.

[31] For a review see T.K. Kuo, J. Pantaleone, *Rev. Mod. Phys.* 61 (1989) 937.

[32] SNO collaboration, *nucl-ex/0204008*. SNO collaboration, *nucl-ex/0204009*.

[33] SNO collaboration, *nucl-ex/0309004*. See also "*HOWTO use the SNO salt flux results*" available at the SNO web site www.sno.phy.queensu.ca.

[34] Super-Kamiokande collaboration, *hep-ex/0205075*.

[35] Gallex collaboration, *Phys. Lett.* B447 (1999) 127. SAGE collaboration, *astro-ph/0204245*. Latest data have been presented in a talk by C. Cattadori at the 'Neutrino 2004' conference (Paris, 14-19 June), web site neutrino2004.in2p3.fr.

[36] The results of the Homestake experiment are reported in B.T. Cleveland et al., *Astrophys. J.* 496 (1998) 505.

[37] KamLAND collaboration, *Phys. Rev. Lett.* 90 (2003) 021802 (*hep-ex/0212021*). KamLAND collaboration, *hep-ex/0406035*.

[38] J.N. Bahcall, S. Basu, M.H. Pinsonneault, *Astrophys. J.* 555 (2001) 990 (*astro-ph/0010346*). A $\chi^2$ for solar data was constructed in G.L. Fogli, E. Lisi, *Astropart. Phys.* 3 (1995) 185.

[39] LUNA collaboration, *nucl-ex/0312015*. See also S. degl'Innocenti et al., *astro-ph/0312559*.

[40] P.C. de Holanda, A. Yu. Smirnov, *hep-ph/0307266*. See also P.C. de Holanda, A. Yu. Smirnov, *hep-ph/0211264*.

[41] P. Creminelli et al., *J. HEP* 05 (052) 2001 (*hep-ph/0102234 updated version 5*).

[42] Sub-MeV solar $\nu_e$ experiments were regarded as the tool for discriminating LMA from the alternative solutions, which have been already excluded. The impact of sub-MeV on still open questions was discussed in A. Strumia, F. Vissani, *J.HEP* 048 (2001) 0111 (*hep-ph/0109172*). Recent analyses find similar results, see e.g. J.N. Bahcall, C. Peña-Garay, *J.HEP* 0311 (2003) 004.

[43] E.G. Adelberger et al., *Rev. of Modern Phys.* 70 (1998) 1265. Recent measurements of $S_{17}(0)$: N. Iwasa et al., *Phys. Rev. Lett.* 83 (1999) 2910. B. Davids et al., *Phys. Rev. Lett.* 86 (2001) 2750. F. Hammache et al., *Phys. Rev. Lett.* 86 (2001) 3985. F. Strieder et al., *Nucl. Phys.* A696 (2001) 219. ISOLDE collaboration, *Phys.Rev. C* 67 (2003) 065805 (*nucl-ex/0212011*). A.R. Junghans et al., *Phys. Rev. C* 68 (2003) 065803 (*nucl-ex/0308003*). K.A. Snover et al., *nucl-ex/0311012*. F. Schumann et al., *Phys. Rev. Lett.* 90 (2003) 232501. For a recent summary see M. Gai, *nucl-ex/0312003*.

[44] P.A. Sturrock, G. Walther, M. S. Wheatland, *Astrophys. J.* 491 (1997) 409. P.A. Sturrock, M. A. Weber, *Astrophys. J.* 565 (2002) 1366. D. O. Caldwell, P. A. Sturrock, *hep-ph/0305303*. A. Milsztajn, *hep-ph/0301252*. P.A. Sturrock, *hep-ph/0309239*. B.C. Chauhan, J. Pulido, *hep-ph/0402194*. See however J. Yoo et al., SK collaboration, *Phys. Rev.* D68 (2003) 092002 (*hep-ex/0307070*) and L. Pandola (GNO collaboration), *hep-ph/0406248*.

[45] See e.g. G.G. Raffelt, *Nucl. Phys.Proc. Suppl.* 110 (2002) 254 (*hep-ph/0201099*); E. Cappellaro, R. Barbon, M. Turatto, *astro-ph/0310859*.

[46] G. G. Raffelt, "*Stars as laboratories for fundamental physics*", Chicago Univ. Press, 1996.

[47] For a recent review see e.g. F. Cei, *Int. J. Mod. Phys.* A17 (2002) 1765 (*hep-ex/0202043*).

[48] H.A. Bethe, *Rev. Mod. Phys.* 62 (1990) 801 and references therein.

[49] A. Burrows, J.M. Lattimer, *Astrophys. J.* 307 (1986) 178.

[50] T.A. Thompson, A. Burrows, P.A. Pinto, *Astrophys. J.* 592 (2003) 434 (*astro-ph/0211194*)

[51] H. Nunokawa, J. T. Peltoniemi, A. Rossi, J. W. F. Valle, *Phys. Rev.* D56 (1997) 1704 (*hep-ph/9702372*).

[52] O.L.G. Peres, A.Yu. Smirnov, *Nucl. Phys.* B599 (2001) 3 (*hep-ph/0011054*).

[53] Neutrino oscillations in SN were discussed in S.P. Mikheev, A.Yu. Smirnov, *Sov. Phys. JETP* 64 (1986) 4. Bounds on sterile oscillations from the SN 1987A rate were discussed in S.P. Mikheev, A.Yu. Smirnov, *JETP Lett.* 46 (1987) 10. T.K. Kuo, J. Pantaleone, *Phys. Rev.* D37 (1988) 298. S.P. Mikheev, A.Yu. Smirnov, *Prog. Nucl. Phys.* 23 (1989) 41. K.Kainulainen, J.Maalampi and J.T. Peltoniemi, *Nucl. Phys.* B358 (1991) 435. H.Athar, J.T. Peltoniemi, *Phys. Rev.* D51 (1995) 5785. A. D. Dolgov, S. H. Hansen, G. Raffelt, D. V. Semikoz, *Nucl. Phys.* B590 (2000) 562 (*hep-ph/0008138*). P. Keranen, J. Maalampi, M. Myyrylainen, J. Riittinen, *hep-ph/0401082*.

[54] X. Shi, G. Sigl, *Phys. Lett.* B323 (1994) 360 (*hep-ph/9312247*).

[55] G.C. McLaughlin, J.M. Fetter, A.B. Balantekin, G.M. Fuller, *Phys. Rev.* C59 (1999) 2873 (*astro-ph/9902106*). D. O. Caldwell, G. M. Fuller, Y. Z. Qian, *Phys. Rev.* D61 (2000) 123005 (*astro-ph/9910175*). J. Fetter, G. C. McLaughlin, A. B. Balantekin, G. M. Fuller, *Astropart. Phys.* 18 (2003) 433 (*hep-ph/0205029*).

[56] Kamiokande-II collaboration, *Phys. Rev. Lett.* 58 (1987) 1490; R.M. Bionta et al., *Phys. Rev. Lett.* 58 (1987) 1494.

[57] J.T. Peltoniemi, *Astronomy and Astrophysics* 254 (1992) 121 first identified the region of large $Deltam_s^2$ (now excluded by the upper bound on the masses by cosmology) where the effect on the shock can be positive.

[58] P. Vogel, J.F. Beacom, *Phys. Rev.* D60 (1999) 053003 (*hep-ph/9903554*); A. Strumia, F. Vissani, *Phys. Lett.* B564 (2003) 42 (*astro-ph/0302055*).

[59] See e.g. C. Lunardini, A. Y. Smirnov, *Nucl. Phys.* B616 (2001) 307 (*hep-ph/0106149*), E. K. Akhmedov, C. Lunardini, A. Yu. Smirnov, *Nucl. Phys.* B643 (2002) 339 and ref.s therein.

[60] H.-T. Janka, W. Hillebrandt, *Astronomy and Astrophysics Supplement Series* 78, 3 (1989) 375. H.-T. Janka, W. Hillebrandt, *Astronomy and Astrophysics* 224 (1989) 49.

[61] M. Th. Keil, G. G. Raffelt, H.-T. Janka, *Astrophys. J.* 590 (2003) 971 (*astro-ph/0208035*).

[62] F.J. Botella, C.S. Lim, W.J. Marciano, *Phys. Rev.* D35 (1987) 896.

[63] K. Takahashi, K. Sato, A. Burrows and T. A. Thompson, *Phys. Rev.* D68 (2003) 113009 (*hep-ph/0306056*).

[64] B. Jegerlehner, F. Neubig, G. Raffelt, *Phys. Rev.* D54 (1996) 1194 (*astro-ph/9601111*).

[65] See e.g. A.Y. Smirnov, D.N. Spergel, J.N. Bahcall, *Phys. Rev.* D49 (1994) 1389 (*hep-ph/9305204*). Even though the title of the paper raises the doubt that large solar mixing is disfavored by SN1987A, it is pointed out that the effect of oscillations in the star can be partially undone by subsequent oscillations in the Earth. This happens for certain values of $\Delta m^2_{\rm sun}$ which are now excluded. Dependence on the initial temperatures has been studied in M. Kachelriess et al., *JHEP* 0101 (2001) 030; M. Kachelriess et al., *Phys. Rev.* D65 (2002) 73016 (*hep-ph/0108100*).

[66] See e.g. G.M. Fuller, A. Kusenko, I. Mocioiu, S. Pascoli, *Phys. Rev.* D68 (2003) 103002 (*astro-ph/0307267*).

[67] A. Kusenko, G. Segre, *Phys. Lett.* B396 (1997) 197 (*hep-ph/9701311*).

[68] J.F. Beacom et al., *Phys. Rev.* D68 (2003) 093005 (*hep-ph/0307025*).

[69] P. Keranen, J. Maalampi, M. Myyrylainen, J. Riittinen, *Phys. Lett.* B674 (2003) 162 (*hep-ph/030704*).

[70] Super-Kamiokande collaboration, *Phys. Rev. Lett.* 90 (2003) 061101 (*hep-ex/0209028*) and references therein. Future improvements are proposed in J.F. Beacom, M.R. Vagins, *hep-ph/0309300*.

[71] Super-Kamiokande collaboration, *Phys. Rev. Lett.* 81 (1998) 1562. Recent detailed results can be found in the thesis by J. Kameda available from the SK web page: www-sk.icrr.u-tokyo.ac.jp/doc/sk/pub. Latest data: talk by M. Shiozawa at the Neutrino 2002 conference, web site neutrino2002.ph.tum.de.

[72] See e.g. K2K collaboration, *hep-ex/0306043*.

[73] MACRO collaboration, *Phys. Lett.* B566 (2003) 35 (*hep-ex/0304037*).

[74] CHOOZ collaboration, *Phys. Lett.* B466 (1999) 415 (*hep-ex/9907037*). CHOOZ collaboration, *hep-ex/0301017*. See also Palo Verde collaboration, *Phys. Rev. Lett.* 84 (2000) 3764 (*hep-ex/9912050*).

[75] Bugey collaboration, *Nucl. Phys.* B434 (1995) 503.

[76] CDHS collaboration, *Phys. Lett.* 134B (1984) 281;

[77] CCFR collaboration, *Phys. Rev. Lett.* 52 (1984) 1384.

[78] NuTeV collaboration, *hep-ex/0110059*. Talks available at www-e815.fnal.gov/NuTeV.html discuss how well simulated spectra agree with data.

[79] Karmen collaboration, *hep-ex/0203021*. For a combined analysis of Karmen and LSND data see E.D. Church et al., *hep-ex/0203023*.

[80] NOMAD collaboration, *Nucl. Phys.* B611 (2001) 3 (*hep-ex/0106102*). CHORUS collaboration, *Phys. Lett.* B497 (2001) 8.

[81] The Monolith proposal is available at www.desy.de/~hoepfner/Neutrino/Monolith. See also G. Rajasekaran, *hep-ph/0402246*.

[82] See e.g. V. Kopeikin, L. Mikaelyan, V. Sinev, *hep-ph/0310246*. See also www.hep.anl.gov/ndk/hypertext/white.html.

[83] C. Bemporad, G. Gratta, P. Vogel, *Rev. Mod. Phys.* 74 (2002) 297 (*hep-ph/0107277*).

[84] H. Nunokawa, O.L.G. Peres, R. Zukanovich Funchal, *Phys. Lett.* B562 (2003) 279 (*hep-ph/0302039*).

[85] D. Michael, *Nucl. Phys. Proc. Suppl.* 118 (2003) 189.

[86] The CNGS project is described at its web site, proj-cngs.web.cern.ch/proj-cngs.

[87] J.M. LoSecco, *hep-ph/0305022*.

[88] Fluka collaboration, *hep-ph/0305208*. For a review see T.K. Gaisser, M. Honda, *Ann. Rev. Nucl. Part. Sci.* 52 (2002) 153 (*hep-ph/0203272*).

[89] N. Okada, O. Yasuda, *Int. J. Mod. Phys.* A12 (1997) 3669 (*hep-ph/9606411*). S.M. Bilenky, C. Giunti, W. Grimus, *Eur. Phys. J.* C1 (1998) 247 (*hep-ph/9607372*). C. Giunti, M. Laveder, *JHEP* 102 (2001) 1 (*hep-ph/0010009*). For recent desperate attempts see M. Sorel et al., *hep-ph/0305255*. V. Barger, D. Marfatia, K. Whisnant, *Phys. Lett.* B576 (2003) 303 (*hep-ph/0308299*).

[90] See e.g. some of the papers in [10] and references therein.

[91] A. Pierce, H. Murayama, *hep-ph/0302131*. C. Giunti, *hep-ph/0302173*.